CB2 cannabinoid receptors modulate HIF-1α and TIM-3 expression in a hypoxia-ischemia mouse model

Elk Kossatz[1], Rafael Maldonado[1] and Patricia Robledo[1, 2]

[1]Laboratory of Neuropharmacology, Pompeu Fabra University, PRBB, Barcelona, Spain

[2]Integrative Pharmacology and Systems Neuroscience, IMIM-Hospital del Mar Research Institute, PRBB, Barcelona, Spain.

Corresponding Authors:
Patricia Robledo, PhD
Integrative Pharmacology and Systems Neuroscience
IMIM-Hospital del Mar Research Institute
PRBB
Calle Dr. Aiguader 88
Barcelona 08003
SPAIN
probledo@imim.es
rafael.maldonado@upf.edu
Tel: +34 93 316 0455
FAX: +34 93 316 0901

Rafael Maldonado, MD, PhD
Laboratory of Neuropharmacology
Pompeu Fabra University
PRBB
Calle Dr. Aiguader 88
Barcelona 08003
SPAIN
rafael.maldonado@upf.edu
Tel: +34 93 316 0824
FAX: +34 93 316 0901

Total word-count: 7393

ABSTRACT

The role of CB2 cannabinoid receptors (CB_2R) in global brain lesions induced by hypoxia-ischemia (HI) insult is still unresolved. The aim of this study was to evaluate the involvement of CB_2R in the behavioural and biochemical underpinnings related to brain damage induced by HI in adult mice, and the mechanisms involved. CB_2R knockout (KO) mice and wild-type littermates (WT) underwent permanent ligation of the left common carotid artery and hypoxia. Behavioural measurements in the rotarod, beam walking, object recognition, open field, and Irwin tests were carried out 24 h, 72 h and 7 days. In KO mice, more extensive brain injury was observed. Behavioural deficits in the Irwin test were observed in both genotypes; while WT mice showed progressive recovery by day 7, KO mice did not. Only KO mice showed alterations in motor learning, coordination and balance, and did not recover over time. A higher expression of microglia and astrocytes was observed in several brain areas of lesioned WT and KO mice. The possible alteration of the inflammatory-related factors HIF-1α and TIM-3 was evaluated in these animals. In both genotypes, HIF-1α and TIM-3 expression was observed in lesioned areas associated with activated microglia. However, the expression levels of these proteins were exacerbated in KO mice in several lesioned and non-lesioned brain structures. Our results indicate that CB_2R may have a crucial neuroprotective role following HI insult through the modulation of the inflammatory-related HIF-1α/TIM-3 signalling pathway in microglia.

Keywords: Hypoxia-ischemia, inflammation, TIM-3, HIF-1α, microglia, motor learning, cannabinoid receptors

1. Introduction

Cerebral ischemia related with stroke, cardiac arrest, cardiovascular surgery, and neurosurgical procedures is one of the major causes of death and disability world-wide, and represents a great burden to society (Flynn et al., 2008). These conditions are often associated with low blood oxygen content (hypoxia), and lead to a complex cascade of events in the brain including oxidative stress, inflammation and neuronal death (Choi et al., 2013). Brain ischemia often leads to death, but those patients who survive show major neurological deficits depending on the area of the brain affected (Kwakkel and Kollen, 2013). Thus, treatment strategies have been focused on pharmacological agents that can help to accelerate recovery of function. Animal models of hypoxia-ischemia (HI) injury can be useful tools to better understand the mechanisms involved in these conditions, and to design more efficacious therapeutic strategies. In this study, we used a model of HI that was originally described by Levine in 1960 to study perinatal and neonatal hypoxia, applying it to adult mice. This model of global hypoxia with unilateral ischemia is relevant in situations in which the brain is deprived of both oxygen content and blood flow, such as cardiac arrest and neurovascular surgeries (Olson and McKeon, 2004). Previous studies using this model in adult mice have shown that HI induces important histopathological and behavioural changes including glial activation, cell death and motor deficits (Olson and McKeon, 2004; Koh et al., 2014; Ashton et al., 2007; Fernandez-Ruiz et al., 2008 and Zhang et al., 2008).

The endocannabinoid system has been studied as a possible target for neuroprotective strategies in ischemia-induced brain damage. This system consists of two main receptors, cannabinoid type 1 receptors (CB_1R) and cannabinoid type 2 receptors (CB_2R), their endogenous ligands, mainly N-arachidonoylethanolamine (anandamide) and 2-arachidonoylglycerol (2-AG) and their corresponding synthesizing and degrading enzymes (Mechoulam and Parker, 2011). CB_1R are highly expressed in the central nervous system (CNS), while CB_2R are mainly localized in immune cells such as lymphocytes, neutrophils and microglia/macrophages (de Fonseca et al., 2005; Pazos et al., 2005), but also in brain neurons (Van Sickle et al., 2005).

Importantly, CB_2R appear to be localized in both astrocytes and microglia (Kearn and Hilliard, 1997; Sheng et al., 2005), and their expression is increased in these types of cells in response to inflammatory stimuli during experimental autoimmune encephalomyelitis (Maresz et al., 2005), and following inflammation associated to ischemic and HI episodes (Ashton et al., 2007; Fernández-Ruiz et al., 2008; Zhang et al., 2008). Various studies have evaluated the neuroprotective role of CB_2R activation following brain damage due to cerebral ischemia. Thus, the CB_2R agonist, trans-caryophyllene suppressed hypoxia-induced cytotoxicity of cultured BV_2 microglia cells through inhibition of NF-κB activation (Guo et al., 2014). In addition, administration of the CB_2R agonists, JWH-133 (Murikinati et al., 2010; Zarruk et al., 2012), O-3853 and O-1966 (Zhang et al., 2007) attenuated infarct volume in mice following middle cerebral artery occlusion (MCAO), although, one study shows that the CB_2R agonist GW405833 does not ameliorate brain damage induced by HI in rats (Rivers-Auty et al., 2014). The beneficial effects of CB_2R agonists were attributed to the inhibition by CB_2R of either neutrophil recruitment (Murikinati et al., 2010), inhibition of leukocyte/endothelial adhesion (Zhang et al., 2007), or to a decrease in microglia/macrophage activation (Zarruk et al., 2012). Only a few genetic studies have evaluated the role of CB_2R in focal ischemia with contradictory results (Murikinati et al., 2010; Zarruk et al., 2012; Zhang et al., 2009). Moreover, the mechanisms involved in the neuroprotective role of CB_2R in global brain injury following HI in adult mice are still largely unknown.

Interestingly, recent findings reveal that HI injury in adult mice, increases the expression of the T-cell immunoglobulin and mucin domain protein (TIM-3) in activated microglia, and this effect is mediated by the hypoxia-inducible factor 1 (HIF-1) (Koh et al., 2015). HIF-1 is a heterodimeric transcriptional regulator of various genes under hypoxic conditions, and has been implicated in inflammatory responses after ischemia (Shi, 2009). TIM-3 is expressed in various immune cell types including microglia, where it modulates adaptive and innate immunity, and is a key promoter of tissue inflammation (Anderson et al., 2007). Since the expression of CB_2R increases in activated microglia (Atwood and Mackie, 2010), and CB_2R regulate microglial activation in pathological conditions (Mecha et al., 2015), we tested the hypothesis that CB_2R may confer neuroprotection after HI through modulation of the HIF-1α/TIM-3 axis.

Therefore, we assessed brain damage in adult WT and CB_2R KO mice subject to HI conditions, and determined the associated behavioural alterations at three different time-points (24 h, 72 h and 7 days) post-insult. In addition, we evaluated the expression levels of astrocytes and activated microglia, as well as the levels of the pro-inflammatory factors, HIF-1α and TIM-3 in activated microglia of several brain structures of both genotypes.

2. Experimental Procedures

2.1. Animals

Homozygote male CB_2R KO mice and WT littermates on a C57BL/6J background (kindly provided by Nancy E. Buckley, Cal State Polytechnic University, Pomona, CA) (Buckley et al., 2000), were bred in the animal facilities of the PRBB. Mice (8 to 15 weeks old) were group-housed and maintained in a temperature (21±1 °C) and humidity (65±10%) controlled room with food and water available *ad libitum*. All the experiments were performed during the light phase of the dark/light cycle (lights on from 08:00 to 20:00 h). Animal procedures were conducted in accordance with the standard ethical guidelines (EU Directive 2010/63/EU for animal experiments), and approved by the local ethical committee (CEEA, PRBB). All experiments were performed under blind conditions. At the end of the experimental procedure, in order to confirm the genotype of the mice, DNA was obtained from the tail. Genotyping was performed routinely by PCR analysis using the following primers: 5'-GGGGATCGATCCGTCCTGTAAGTCT-3' (CB_2KO forward); 5'-GGAGTTCAACCCCATGAAGGAGTAC-3' (WT forward); 5'-GACTAGAGCTTTGTAGGTAGGCGGG - 3' (WT and CB_2KO reverse).

2.2. Surgery

Mice were randomly assigned to either the sham-operated group or the HI groups. The HI procedure was adapted from a previously described methodology (Levine, 1960; Rice et al., 1981). Briefly, mice were anesthetized with isoflurane (mixture of O_2 and N_2O (0.3/0.7 L/min), and placed on a heat plate to maintain a constant body temperature of 37 °C during the surgery. A median incision in the neck was performed exposing the left common carotid artery, which was then isolated from nerve and vein to permanently

ligated it in two locations with 4-0 surgical silk. The carotid artery was not severed in order to prevent possible death from haemorrhage. The ligature was placed just proximal to the bifurcation of the common carotid artery into the internal and external carotid artery. The wound was then sutured, and the animals were returned to their cages. Hypoxic episodes were conducted 60 min after left common carotid artery occlusion, when the animals had recovered from anaesthesia and presented normal behaviours. A hypoxia chamber (BioSpherix, NY, USA) was used to conduct hypoxic episodes consisting of a constant flow of 10% oxygen for 60 min. The temperature of the mice (37 ºC) was maintained inside the chamber via heating devices placed beneath the animal cage. Sham-operated animals received common carotid artery isolation, but no ligation or hypoxia was performed. After the HI episode, mice were allowed free access to food and water. Body temperature was measured before and after surgery, and before and after hypoxia by using a mouse rectal probe. Sixty seven WT and 58 KO mice followed the HI procedure, while 17 WT and 14 KO mice were sham-operated controls.

2.3. Behavioural tests

In order to evaluate the behavioural, motor and cognitive alterations associated with HI, sham-operated and HI mice were tested in the rotarod, the beam-walking, the open field and the Irwin test 24 h, 72 h and 7 days after the procedure. Cognitive performance was tested 72 h and 7 days after HI using the novel object recognition test (NOR). All of the tests were conducted by observers blind to the experimental conditions.

Irwin test. Mice were placed in a Plexiglas cylinder and a modified Irwin test (Irwin, 1968) was conducted to evaluate subjective signs of behavioural dysfunction produced by HI and the sham operation. Several symptoms were evaluated by their presence or absence (loss of balance, ptosis and loss of traction) on a 1 point scale. Other symptoms were rated on a 2-point scale (abnormal gait, piloerection, low reactivity to touch), and neurological deficits rated on a scale from 0-2 (no deficit = 0, forelimb weakness and torso turning to the affected side when held by de tail = 1, or circling to affected side = 2). The final score was expressed by the sum of all symptoms observed in each animal (Total from 0 to11).

Open field test. Mice were placed in an experimental arena (Plexiglas box, 90x70) in order to evaluate locomotor activity, and the total distance travelled was determined by counting the number of squares crossed (units) during a 5 min period.

Rotarod test. The accelerating rotarod (Panlab) was used to evaluate motor coordination. Mice were trained for 2 days before HI. Each training day consisted of 60 sec at 6 rpm (day 1) and 60 sec at 8 rpm (day 2). The test day consisted of 5 trials using the rotarod in acceleration mode from 4 rpm to 20 rpm until the animal fell from the rod. The latency to fall off the rod on every trial was determined, and the mean of the 5 trials was used in the data analysis.

Beam-walking test. To evaluate motor coordination and balance, the beam-walking test was performed. This test examines the ability of the animal to remain upright and to walk on an elevated beam with varying thicknesses. The beams consisted of 1-m long strips of wood with 20 or 6 mm square cross sections. The beams were placed horizontally, 40 cm above the floor, with one end mounted on a support and the other end attached to the home cage of the animal as the escape box. Mice were trained for 2 days before HI. Each training day consisted in the animal traversing the 20 mm square beam (2 trials) and on the test day, mice traversed a narrower beam of 6 mm. The latency to traverse the beam was determined, and the analysis was based on the mean scores of the two trials.

Novel object recognition test (NOR). In this paradigm, a black Plexiglas maze with two corridors (30 cm long x 4.5 cm wide, and 15 cm high walls) set at a 90° angle (Panlab) was used. First, mice were habituated to the empty maze for 9 min. Twenty-four h later, mice were place back in the maze for another 9 min, but this time two identical objects were presented, one on each arm of the maze, and the time that the mice spent exploring each object was recorded. The mice were again placed in the maze 3 h later for 9 min, but one of the familiar objects was replaced with a novel object, and the total time spent exploring each object (novel and familiar) was recorded. Object exploration was defined as the orientation of the nose to the object at a distance of less than 2 cm. A discrimination index was calculated as the time spent exploring the novel object minus the time exploring the familiar object divided by the total time exploring both objects. A higher discrimination index is considered to reflect greater memory retention.

2.4. Histological analysis

The extent of the lesion was visualized using a standard Cresyl violet staining protocol. With this procedure the infarct area can be identified by the loss of Nissl staining in the HI ipsilateral hemisphere. One group of mice (see Supp. Table 1) were euthanized by cervical dislocation, and fresh brains were harvested and sliced at 20 µm with a cryostat and mounted onto gelatin-coated slides and stored at -80 °C. Brain slices were divided into 5 parallel series from 1.98 to 1.34 , from 1.18 to 0.38, from -0.22 to -0.88, from -1.46 to -2.06 and from -2.30 to -2.96 relative to Bregma (Paxinos and Franklin, 2001). The stained sections of the brain were analysed at 1x (zoom factor 0.8x) using an Olympus MVX10 Macro Zoom Microscope equipped with Olympus DP71 digital camera. The ischemic lesion was delimited using the ImageJ software. For each mouse, the lesioned area was calculated in 5 brain sections, and the sum in pixels was transformed to μm^2 and expressed as a percentage of the contralateral hemisphere in order to correct for possible oedema in the ipsilateral hemisphere (Rousselet et al., 2012).

To determine the expression levels of glial fibrillary acid protein (GFAP) and Iba-1 in different brain areas, we performed immunohistochemistry in a different group of mice (see Supp. Table 1). Mice were deeply anesthetized by intraperitoneal injection (0.2 ml per 10 g body weight) of a mixture of ketamine (100 mg per kg) and xylazine (20 mg per kg), and intracardially perfused with 4% paraformaldehyde in 0.1 M phosphate buffer (pH 7.5), delivered with a peristaltic pump. Brains were post-fixed overnight at 4 °C in the same fixative solution and cryoprotected in a solution of 30% sucrose at 4ºC during 24 h. Brain sections were sliced at 30 µm with a microtome and stored at 4ºC in a solution containing 5% sucrose and 0.02% sodium azide in 0.1 M phosphate buffer. Free floating coronal sections from 1.18 to 0.38 and from -1.46 to -2.06 relative to Bregma were collected to determine the expression of glial fibrillary acid protein (GFAP) and Iba-1 in motor cortex, striatum and hippocampus. In addition, brain sections were stained with Cresyl violet to determine the extent of lesions in these mice. The immunohistochemical procedure was adapted from a previously described methodology (Blanco-Calvo et al., 2014). Briefly, the sections were placed in a blocking solution containing 10% normal goat serum, 0.3% triton X-100, and 0.1% sodium azide in PBS for 1 h, incubated overnight in the following diluted primary antibodies at 4°C: rabbit anti-GFAP (1:500, Dako; cat. #Z0334) or rabbit anti-Iba1 (1:500, Wako; cat. no. 019-19741). On day two,

sections were incubated with biotinylated goat anti-rabbit IgG (1:500, Vector; cat. no.BA-1000), and ExtrAvidin peroxidase (Sigma, cat. no. E2886) diluted 1:2000 at room temperature for 1 h. Immunolabeling was revealed with 0.05% DAB (Sigma), 0.05% nickel ammonium sulphate, and 0.03% H_2O_2 in PBS. Sections were mounted and analysed at 20x using a Leica DMR microscope equipped with a digital camera Leica DFC 300FX. Three images per structure were analysed in order to quantify manually GFAP and Iba-1 cells expression using ImageJ software (NIH). The mean number of cells per mm^2 was plotted for motor cortex, striatum and hippocampus in WT and KO mice.

To determine the expression levels of TIM-3, HIF-1α and Iba-1 in different structures of the brain, immunofluorescence studies were carried out as previously described (Cutando et al., 2013). Free-floating slices were placed in 0.3% Triton X-100, 10% donkey serum (Sigma) in PB, and incubated overnight at 4°C with the following primary antibodies: anti- HIF-1α (1: 200, Abcam; cat. no. ab16066), anti-Iba-1 (1:500, Wako; cat. no. 019-19741) and anti-TIM-3 (1:500, R&D systems, cat. no. AF1529). The following day, sections were incubated for 2 h at room temperature with Alexa 647 donkey anti-mouse-IR, Alexa 488 donkey anti–rabbit-Cy2 and Alexa 555 donkey anti-goat-Cy3 (1:500; Invitrogen/ Molecular Probes), and mounted. Confocal images were obtained using a Leica TSC SP8 confocal microscope at 20X with a 1.5 zoom increase. Eighteen images of stained sections (from Bregma +1.18 mm to Bregma –2.30 mm) were analysed using ImageJ software (NIH) in order to manually quantify the expression of Iba-1/TIM-3, and Iba-1/HIF-1α. Positive cells in each structure were averaged and compared between genotypes.

2.5. Morphological analysis of activated microglia

To assess whether the reactive microglia observed following HI in WT and KO mice presented differential morphologies, we analysed the Iba-1 immunostained sections using the methodology previously reported (Lopez-Rodriguez et al., 2015). Cells were classified according to five types: Type I, cells with two or less cellular processes; Type II, cells showing 3 to 5 short branches; Type III, cells with more than 5 and longer processes and small cell bodies; Type IV, cells with large somas and retracted, thicker processes; Type V, cells with amoeboid cell bodies and many short processes. Reactive microglia (Types III, IV and V) cells

were counted in the hippocampus, the striatum and the motor cortex of WT and KO lesioned mice by visual inspection of the images obtained from stained sections showing Iba-1 positive cells. We then grouped cell types I, II, III and IV that correspond to an M2 (anti-inflammatory) phenotype, and cell type V to an M1 (pro-inflammatory) phenotype (Franco and Fernández-Suárez, 2015).

2.6. Statistical analyses

The behavioural data were analysed using repeated measures ANOVA with time (24 h, 72 h and 7 days) as within subjects factor, genotype (CB_2R KO and WT mice), and lesion (lesioned, non-lesioned) as between subject factors, followed by the Fisher's LSD *post-hoc* test for multiple comparisons when appropriate. The mortality and variability (lesion vs. non-lesion) ratios were evaluated with the χ-square non-parametrical test. The extent of the lesion was analysed using the Student's t-test. The immunohistochemistry data and the morphological characteristics of microglial cells were analysed using a two-way ANOVA with genotype and lesion or genotype and cell type as between subject factors followed by a Fisher's LSD *post-hoc* when appropriate. The immunofluorescence results were analysed between genotypes using one-way ANOVA. Correlations between TIM-3/Iba-1 expression and behavioural outcomes were analysed using the Spearman correlation test. All data were expressed as the mean + S.E.M. A p-value below 0.05 was considered statistically significant. The statistical analyses were performed with the "Statistica" programme, version 6 (StatSoft Inc.), except for correlations, where the GraphPad Prism software was used (GraphPad Software).

3. Results

3.1. Mortality and severity of the lesion in WT and CB_2R KO mice following HI

Twenty out of 67 WT and 10 out of 58 CB_2R KO mice did not survive following the HI procedure. Most deaths in WT and KO mice occurred on the day of the surgery during the hypoxia procedure and it was not possible to extract the brains in time to visualize any differences between genotype in the extent of the brain lesion. Among those mice that survived the HI procedure, there were 3 KO mice that died 1, 3 and 5 days following HI, and 2 WT mice that died 1 and 2 days after HI. Although a higher percentage of WT

than KO mice died (30% in WT vs. 17% in KO mice), no significant differences in mortality ratio were observed between genotypes. Two different types of animals survived: those that exhibited lesions in the ipsilateral hemisphere to the carotid ligation, and those that did not show overt lesions. In WT, 13 out of 47 mice were lesioned, and 34 out of 47 mice showed no apparent infarct. In KO animals, 26 out of 48 mice were lesioned, while 22 out of 48 mice were not lesioned. Thus, a greater percentage of CB_2R KO mice showed lesions as compared to WT mice (54% in KO vs. 28% in WT mice; $p < 0.01$, χ^2 test).

HI-induced brain damage ipsilateral to the carotid ligation was observed in WT mice in hippocampal areas CA1, CA2 and CA3, and in the sensory, entorhinal and piriform cortices (Fig. 1C). In CB_2R KO mice, more extensive brain injury was observed including the hippocampus, sensory, entorhinal, piriform and motor cortices, the dorsal striatum, the Globus pallidus and the amygdala (Fig. 1F). Accordingly, CB_2R KO mice showed higher overall brain damage than WT mice (27 % in KO vs. 12 % in WT mice; **p<0.01**) (Figure 1G). The contralateral hemisphere remained intact in both genotypes. In sham and HI non-lesioned mice of both genotypes, no overt signs of brain injury were observed in either hemisphere (Fig. 1).

3.2. CB_2R KO mice show greater behavioural, motor coordination and balance deficits than WT mice following HI

To assess behavioural, motor coordination, and balance deficits we used the Irwin, the rotarod, the open field, and the beam walking tests. Six groups of mice were included in these studies: three groups of WT mice (13 lesioned, 34 non-lesioned and 17 sham-operated), and three groups of KO mice (26 lesioned, 22 non-lesioned and 14 sham-operated).

Qualitative symptoms of behavioural dysfunction were evaluated 24 h, 72 h and 7 days following HI using the Irwin test (Fig. 2A). Repeated measures ANOVA revealed a significant main effect of time of testing ($F(2,202)=35.1$, $p<0.001$), and lesion ($F(2,101)=25.4$, $p<0.001$), but no significant main effect of genotype. Significant interactions were observed between time and genotype ($F(2,202)= 7.4$, $p<0.001$), and time and lesion ($F(4,202)=11.7$, $p<0.001$). Post-hoc analysis 24 h after HI showed a significant increase in symptoms in WT lesioned ($p<0.001$) and non-lesioned ($p<0.05$) mice with respect to sham-operated WT animals, and in KO lesioned mice with respect to sham-operated KO mice ($p<0.001$). At 72 h, both WT

and KO mice showed signs of dysfunction with respect to their respective control groups ($p<0.05$). At 7 days post-insult, only KO lesioned mice showed deficits with respect to controls ($p<0.05$). These data indicate that WT mice progressively recover functionality, while KO mice show persistent symptoms of behavioural dysfunction even 7 days after HI insult.

In the rotarod test, deficits were observed 24 h, 72 h and 7 days following HI (Fig. 2B). Repeated measures ANOVA revealed a significant effect of time ($F(2,218)=21.1$. $p<0.001$), genotype ($F(1,109)=15.9$, $p<0.001$), and interaction between genotype and lesion ($F(2,109)=8.4$, $p<0.001$), and between time and genotype ($F(2,218)=6.0$, $p<0.01$). Post-hoc analysis at 72 h and 7 days showed a significant decrease in fall latency in KO mice with respect to sham-operated controls ($p<0.05$), and with respect to WT lesioned mice ($p<0.001$). No significant deficits in performance were observed at any time point in WT lesioned mice or in non-lesioned mice of either genotype.

In the beam walking test, deficits were observed in KO mice at 24 h, 72 h and 7 days following HI (Fig. 2C). Repeated measures ANOVA revealed a significant effect of time ($F(2,214)=28.1$, $p<0.001$), genotype ($F(1,107)=4.6$, $p<0.05$), lesion ($F(2,107)=6.0$, $p<0.01$), and interactions between genotype and lesion ($F(2,107)=6.2$, $p<0.01$), time and lesion ($F(4,214)=5.2$, $p<0.001$), and between time, genotype and lesion ($F(4,214)=2.4$, $p<0.05$). Post-hoc analysis 24 h after HI showed a significant increase in arrival latency in KO ($p<0.001$) with respect to sham-operated KO mice ($p<0.001$), and lesioned WT mice ($p<0.01$). At 72 h, KO lesioned mice showed a significant increase in arrival latency with respect to sham-operated controls ($p<0.05$). At 7 days following HI, KO lesioned mice still showed some non-significant deficits with respect to sham-operated control mice. No significant deficits were observed at any time point in WT lesioned mice or in non-lesioned mice of either genotype.

In the open field test, both WT and KO lesioned mice showed slight non-significant decreases in locomotor activity 24 h following HI, which recovered at 72 h and 7 days post-insult (Fig. 2D).

In the NOR test (WT: 7 lesioned, 22 non-lesioned and 8 sham-operated; KO: 15 lesioned, 16 non-lesioned and 7 sham-operated) mice were evaluated. Robust memory deficits were observed 72 h and 7 days following HI in both WT and KO lesioned mice (Fig. 2E). Repeated measures ANOVA revealed a

significant main effect of lesion ($F(2,61)=38.7$, $p<0.001$), indicating that lesioned mice of both genotypes showed deficits in recognition memory with respect to sham-operated controls, but no significant differences were observed between genotypes or time of testing.

3.3. Increased glial expression in the cortex, striatum and hippocampus of WT and CB_2R KO mice following HI

The analysis of GFAP and Iba-1 positive cells was carried out in 7 WT and 8 KO lesioned, 7 WT and 7 KO non-lesioned, and 7 WT and 7 KO sham-operated mice. Following HI, GFAP expression was increased in the ipsilateral hemisphere of WT and KO mice with respect to the contralateral hemisphere in the motor cortex (Fig. 3A), striatum (Fig. 3B) and hippocampus (Fig. 3C). In the motor cortex, statistical analysis revealed a significant effect of lesion ($F(2,35)=15.1$, $p<0.001$), but no significant effect of genotype or interaction between factors. Similarly, in the striatum a significant effect of lesion ($F(2,32)=12.0$, $p<0.001$), but no significant effect of genotype or interaction between factors were observed. Finally, in the hippocampus, statistical analysis revealed a significant effect of lesion ($F(2,31)=55.9$, $p<0.001$), but no significant effect of genotype or interaction between factors.

Iba-1 expression was increased in ipsilateral lesioned areas of the motor cortex (Fig.3D), striatum (Fig 3E) and hippocampus (Fig. 3F) of WT and KO mice compared to the contralateral hemisphere following HI. In the motor cortex, a significant effect of genotype ($F(1,33)=4.8$, $p<0.05$), lesion ($F(2,33)=6.3$, $p<0.01$), but no significant interaction between factors were observed. Similarly, in the striatum, a significant effect of lesion ($F(2,35)=26.8$, $p<0.001$), but no significant effect of genotype or interaction between factors were revealed. In the hippocampus however, a significant effect of genotype ($F(1,34)=5.6$, $p<0.05$), lesion ($F(2,34)=111.9$, $p<0.001$), and interaction between factors ($F(2,34)=6.6$, $p<0.01$) were found. The post-hoc test showed a significant increase in Iba-1 expression in WT ($p<0.001$) and KO ($p<0.001$) lesioned mice with respect to sham-operated animals. In addition, KO lesioned mice showed higher Iba-1 expression than WT lesioned mice ($p<0.001$).

To analyse the morphology of the activated microglia observed in lesioned WT (n=7) and CB_2R KO (n=8) mice, we classified these cells into morphological types I, II III and IV (M2, anti-inflammatory), or type V

(M1, pro-inflammatory) phenotype (Supp. Fig. 1). The results showed a similar number of pro- and anti-inflammatory associated phenotype in the hippocampus in both WT and KO mice. Statistical analysis revealed a significant effect of cell type in the motor cortex ($F(1,13)= 195.8$, $p<0.001$) and in the striatum ($F(1,13)=44.8$, $p<0.001$), indicating more anti-inflammatory than pro-inflammatory cells in both genotypes.

3.4. Increased HIF-1α expression in microglia of WT and CB_2R KO mice following HI

To evaluate the HIF-1α expression in microglia in different brain structures following HI, we performed double immunofluorescence studies (Iba-1 and HIF-1α) in brain sections of WT and CB_2R KO mice, and two different analyses were performed. One analysis including the total size group of WT and KO lesioned mice (7 WT: mean ± S.E.M. lesion size = 9 ± 1.76%, and 9 KO: mean ± S.E.M. lesion size = 27% ± 7.03; $p<0.05$) (Fig. 4 A-E and 5 A-D), and another analysis considering only similar moderate lesion size sub-groups (7 WT: mean ± S.E.M. lesion size = 9% ± 1.76, and 7 KO mean ± S.E.M. lesion size = 14% ± 1.75; n.s.) (Fig. 4 F-J and 5 E-H). The criteria used to consider a moderate lesion was less than 27% of lesioned area with respect to the contralateral hemisphere.

In the total size group analysis, higher expression levels of HIF-1α in microglia were observed in lesioned areas of KO with respect to WT mice in the ipsilateral entorhinal cortex ($F(1,9)=6.6$, $p<0.05$) (Fig. 4A), amygdala ($F1,10)=5.1$, $p<0.05$) (Fig. 4B), hippocampus ($F(1,10)= 11.5$, $p<0.01$) (Fig. 4C), motor cortex ($F(1,12)=13.4$, $p<0.01$) (Fig. 4D), and striatum ($F(1,13)=9.6$, $p<0.01$) (Fig. 4E) In non-lesioned areas, higher expression levels in KO with respect to WT mice were found in olfactory tubercle ($F(1,11)= 8.0$, $p<0.05$) (Fig. 5A), nucleus accumbens ($F(1,12)=12.2$, $p<0.01$) (Fig. 5B), lateral septum ($F(1,10)= 7.1$, $p<0.05$) (Fig. 5C) and thalamus ($F(1,11)=6.4$, $p<0.05$) (Fig. 5D).

In the similar moderate lesion size sub-groups, higher expression levels of HIF-1α in microglia were observed in lesioned areas of KO with respect to WT mice in the ipsilateral entorhinal cortex ($F(1,8)=7.2$, $p<0.05$) (Fig. 4F), hippocampus ($F(1,8)=6.1$, $p<0.05$) (Fig. 4H), motor cortex ($F(1,10)=8.3$, $p<0.05$) (Fig. 4I), and striatum ($F(1,11)=9.0$, $p<0.05$) (Fig. 4J). In non-lesioned areas, higher expression levels in KO

with respect to WT mice were found in olfactory tubercle ($F(1,10)= 6.9$, $p<0.05$) (Fig. 5E), nucleus accumbens ($F(1,10)=8.8$, $p<0.05$) (Fig. 5F) and lateral septum ($F(1,8)= 9.9$, $p<0.05$) (Fig. 5G).

3.5. Increased TIM-3 expression in microglia of WT and CB_2R KO mice following HI

To determine the expression of TIM-3 in microglia in different brain structures following HI, we performed double immunofluorescence studies (Iba-1 and TIM-3) in brain sections of WT and CB_2R KO mice. Two different analyses were performed as described before. The analysis including the total size group of WT and KO lesioned mice was carried out in 7 WT and 10 KO mice (Figs. 6 A-D , 7 A-B and 8 A-D), and the analysis including similar moderate lesion size sub-groups was performed in 7 WT and 7 KO mice (Figs. 6 E-H , 7 C-D and 8 E-H).

In the total size group analysis, higher expression levels of TIM-3 in microglia were revealed in lesioned areas of KO with respect to WT mice in the ipsilateral sensory cortex ($F(1,14)=31.7$, $p<0.001$) (Fig. 6A), entorhinal cortex ($F(1,13)=18.4$, $p<0.001$) (Fig. 6B), amygdala ($F1,12)=4.9$, $p<0.05$) (Fig. 6C), hippocampus ($F(1,13)= 8.5$, $p<0.05$) (Fig. 6D), motor cortex ($F(1,14)=5.0$, $p<0.05$) (Fig. 7A) and striatum ($F(1,15)=7.0$, $p<0.05$) (Fig. 7B). In non-lesioned areas, higher expression levels in KO with respect to WT mice were revealed in the olfactory tubercle ($F(1,14)= 4.7$, $p<0.05$) (Fig. 8A) and lateral septum ($F(1,15)= 6.4$, $p<0.05$) (Fig. 8C). No significant effects of genotype were observed in nucleus accumbens or thalamus (Fig. 8 B, D).

In the similar moderate lesion size sub-groups, higher expression levels of TIM-3 in microglia were observed in lesioned areas of KO with respect to WT mice in the ipsilateral sensory cortex ($F(1,12)=8.1$, $p<0.05$) (Fig. 6E), and entorhinal cortex ($F(1,11)=19.1$, $p<0.01$) (Fig. 6F), amygdala ($F1,9)=6.0$, $p<0.05$) (Fig. 6G) and hippocampus ($F(1,11)=5.6$, $p<0.05$) (Fig. 6H). In non-lesioned areas higher expression levels in KO with respect to WT mice were observed in the lateral septum ($F(1,12)= 9.5$, $p<0.01$) (Fig. 8G). No significant effects of genotype were observed in motor cortex, striatum, olfactory tubercle, nucleus accumbens or thalamus (Figs. 7C, D and 8E, F, H).

3.6. Correlations between behavioural output and extent of the lesions and TIM-3/Iba-1 expression levels

Since brain injury and inflammation following HI was observed in several areas of the brain, we tested the hypothesis that particular behavioural alterations would be related to the extent of the lesion and to inflammatory processes in specific brain structures. Thus, we performed correlation analyses in WT and KO mice between behavioural alterations 7 days after the HI insult and the extent of the lesions, and TIM-3/Iba-1 expression levels in different brain structures (Fig. 9). Behavioural deficits in the Irwin test (symptoms) were positively correlated with greater brain damage ($R= 0.51$, $p<0.001$), and with higher TIM-3/Iba-1 co-expression in the thalamus ($R= 0.66$, $p<0.05$), and the overall brain ($R= 0.51$, $p<0.05$) (Fig. 9A). Behavioural deficits in the rotarod test (decreased fall latency) were significantly correlated with greater brain damage ($R= -0.55$, $p<0.001$), and with higher TIM-3/Iba-1 co-expression in the motor cortex ($R=-0.63$, $p<0.05$), overall cortical areas ($R=-0.73$, $p<0.01$), striatum ($R=-0.58$, $p<0.05$), nucleus accumbens ($R=-0.66$, $p<0.01$), and amygdala ($R=-0.60$, $p<0.05$) (Fig. 9B). Alterations in the beam walking test (increased arrival latency) were significantly correlated with greater brain damage ($R= 0.54$, $p<0.001$), and with higher TIM-3/Iba-1 co-expression in the olfactory tubercle ($R= 0.53$, $p<0.05$) (Fig. 9C). No significant correlations were observed in the hippocampus or the lateral septum with any of the behavioural deficits exhibited by WT and KO mice after HI.

4. Discussion

CB_2R KO mice exhibited more extensive brain lesions than WT mice following HI insult, attaining most of the ipsilateral cortex and hippocampus, and even reaching parts of the striatum and amygdala. Accordingly, CB_2R KO mice showed persistent behavioural alterations and deficits in motor learning, coordination and balance. Cognitive performance was severely impaired in both genotypes, and no recovery was observed over time. A significantly higher expression of microglia was observed in the hippocampus of lesioned CB_2R KO with respect to WT mice. TIM-3 expression in microglia was also more extensive in CB_2R KO than in WT mice, and was detected in more medial non-lesioned areas such as the thalamus, olfactory tubercle, nucleus accumbens and septum. Likewise, HIF-1α expression was also

higher in lesioned areas of CB_2R KO compared to WT mice, including the hippocampus, amygdala, motor and entorhinal cortices and striatum, but also in several non-lesioned structures such as the olfactory tubercle, the nucleus accumbens, septum and thalamus.

Finally, TIM-3/Iba-1 expression in several brain structures significantly correlated with behavioural, motor learning, coordination and balance deficits. These results indicate that CB_2R may modulate inflammatory factors such as TIM-3 following brain damage due to HI insult, and consequently prevent associated behavioural, motor learning, coordination and balance deficits.

To investigate the involvement of CB_2R in global brain injury following HI, we used a new genetic model using CB_2R KO and WT adult mice subjected to a permanent unilateral common carotid artery occlusion followed by hypoxic conditions. Following this procedure, HI produced moderate mortality and variable brain damage, as previously reported (Olson and McKeon, 2004). Although mortality was higher in WT than CB_2R KO mice, no significant differences were found between genotypes. Nonetheless, we cannot rule out that more WT mice died due to more extensive lesions than KO mice. However, this is unlikely since most WT and KO mice died during the HI procedure. In mice that survived, two populations could be observed with regards to brain lesion characteristics: mice exhibiting neuronal damage in the ipsilateral hemisphere, and mice exhibiting no overt lesions in any of the two hemispheres. This fact may be due to individual differences in posterior communicating arteries that form part of the circle of Willis in mice, which have been shown to affect lesion volume in multiple models of cerebral ischemia (Sheng et al., 1999; Wellons III et al., 2000; Yonekura et al., 2004). The percentage of animals with lesions was significantly higher in the CB_2R KO (54 %) than in the WT (28 %) group, which could be due to a disparate cerebral vascularisation in both genotypes. However, there is no data to support this hypothesis. In addition, there are no studies thoroughly assessing the nature or extent of brain damage occurring in mice lacking CB_2R following HI-induced brain injury. In this study, WT lesioned mice displayed restricted neuronal damage mainly in the hippocampus, with some animals also showing lesions in the sensory, entorhinal or piriform cortices. These results confirm previous evidence regarding the susceptibility of these mouse brain areas to be injured after HI (Olson and McKeon, 2004). On the other hand, CB_2R KO mice showed a larger infarct area at the level of the hippocampus, sensory, entorhinal and piriform cortices, and in addition,

damage tissue also comprised the motor cortex, striatum and amygdala. These findings suggest that CB_2R play a general protective role in adult mice subject to HI by preventing a more widespread lesion in the brain.

To examine the behavioural consequences of HI, we determined a general behavioural score in the Irwin test, as well as motor and cognitive performance in WT and CB_2R KO mice 24 h, 72 h and 7 days following this procedure. Behavioural deficits were observed in both genotypes 24 h after HI. However, whereas WT mice recovered over time, CB_2R KO mice did not, indicating that CB_2R are involved in the restoration of function following HI insults. Motor skill learning, coordination and balance were selectively impaired in CB_2KO mice, and no recovery was observed over time. These effects were not due to impaired locomotor activity since distance travelled in the open field was only slightly affected in all the experimental groups. Previous studies have reported neuroprotective effects of CB_2R activation in other animal models. Thus, the administration of a dual CB1/CB2 receptor agonist, KN38-7271 in rats (Schmidt et al., 2012), or the selective CB_2R agonist, O-1966 in mice (Zhang et al., 2009) reduces motor learning impairments induced after MCAO, and the overexpression of CB_2R confers neuroprotection against 6-OHDA-induced lesions of the mouse striatum (Ternianov et al., 2012).

Cognitive function was evaluated using the object recognition test 3 and 7 days following HI. Both WT and CB_2R KO lesioned mice showed severe memory impairments on both testing days. Contrary to the other behaviours studied, the cognitive deficit found in WT mice was not enhanced in CB_2KO mice, probably due to a ceiling effect that prevented further deficits to be observed in these mice. These results are consistent with the extensive damage induced by HI to the hippocampus in both genotypes, and reveal that even unilateral lesions of this structure are sufficient to profoundly affect cognitive function in mice subjected to these adverse conditions.

We found that the expression of reactive astrocytes was greater in the ipsilateral motor cortex, the striatum and hippocampus of WT and CB_2R KO mice subjected to HI with respect to sham-operated controls. Astrocytes are thought to promote brain repair following traumatic brain injury and stroke conditions, and are up-regulated under HI conditions in the ipsilateral cerebral cortex of mice (Koh et al., 2015; Olson and McKeon, 2004). Furthermore, microglia was also increased in the ipsilateral motor cortex, the striatum of

WT and CB_2R KO mice following HI with respect to sham-operated controls. In the hippocampus however, CB_2R KO mice showed higher expression levels than WT mice. Microglia, which are the main resident immune cells in the brain, are up-regulated following HI episodes (Koh et al., 2015; Olson and McKeon, 2004). They produce inflammatory mediators (Woodroofe et al., 1991) that contribute to cell death and increased infarct size. Nonetheless, it has been demonstrated that microglia can adopt an alternative phenotype changing from the classical pro-inflammatory M1 to an M2 anti-inflammatory phenotype (Franco and Fernández-Suárez, 2015). Moreover, CB_2R have been implicated in the transformation of microglia to a more protective phenotype (Mecha et al., 2015). Thus, we carried out morphological analyses of microglial cells in WT and KO mice to determine genotype differences in microglial phenotype. This evaluation showed that in areas where brain injury was extensive such as the hippocampus, no differences in the number of cell types I, II, III and IV (anti-inflammatory phenotype), and cell type V (pro-inflammatory phenotype) were observed in either genotype. In contrast, in areas where brain damage was sparse such as the motor cortex and the striatum, more type I, II, III and IV than type V morphologies were found in both WT and KO mice. These findings agree with the dual role (pro- and anti-inflammatory) of microglia following HI conditions (Franco and Fernández-Suárez, 2015) by showing that in salvageable tissue the protective microglial phenotype is more abundant. However, CB_2R do not seem involved in this differential effect of microglia cells.

In order to determine the possible mechanisms involved in these responses of CB_2R, we evaluated in WT and KO mice the expression of the pro-inflammatory factor HIF-1α in activated microglia, which is rapidly increased in the cell nucleus following systemic hypoxia, and may contribute to tissue damage (Shi et al., 2009). Because HIF-1α appears mostly to be induced following ischemia in the penumbral tissue, we examined both lesioned and non-lesioned structures in WT and KO mice. We found that HIF-1α expression was higher in lesioned areas of CB_2R KO compared to WT mice, including the hippocampus, amygdala, motor and entorhinal cortices and striatum, but also in several non-lesioned structures such as the olfactory tubercle, the nucleus accumbens, septum and thalamus. These findings suggest that CB_2R may be limiting the detrimental action of HIF-1α under HI to prevent brain damage. Similarly, we also found that the co-expression of TIM-3 and Iba-1 immunofluorescence was exacerbated in CB_2R KO with

respect to WT mice in lesioned areas (hippocampus, amygdala, motor and entorhinal cortices and striatum), but also in non-damaged areas (olfactory tubercle and lateral septum). These findings are consistent with recent evidence associating the HIF-1/glial TIM-3 axis with inflammation and brain damage to the cerebral cortex following HI insults (Koh et al., 2015). Our data indicate that the inflammatory process, which results from brain injury after HI is more important in mice lacking CB_2R, covering more medial areas. Importantly, the increase in HIF-1α and TIM-3 in KO mice with respect to WT mice was also observed when we compared animals with similar lesions, especially in entorhinal cortex, hippocampus and septum. These results suggest that HIF-1α and TIM-3 expression is not a consequence of a more extensive lesion size in KO mice, but it is probably due to the lack of CB_2R. Moreover, these findings demonstrate for the first time the role of these receptors in the modulation of the pro-inflammatory factors, HIF-1α and TIM-3, which may underlie this neuroprotective role of CB_2R. Previous reports have shown that pharmacological activation of CB_2R reduces brain damage in the MCAO ischemia model by inhibiting neutrophil recruitment (Murikinati et al., 2010) or by decreasing microglia/macrophage activation (Zarruk et al., 2012). These data, together with recent evidence showing that blockade of TIM-3 reduces neutrophil recruitment by glial cells, and diminishes IL-1β and CXCL1 (Koh et al., 2015), supports our hypothesis that CB_2R play a crucial role in modulating the HIF-1α/TIM-3 axis in microglia to prevent widespread inflammation and global brain damage following HI insults.

Behavioural alterations were significantly associated with greater brain damage and increased expression of TIM-3 in microglia. In the Irwin test, behavioural deficits were observed at 24 and 72 h following HI in both WT and CB_2R KO lesioned mice. However, while WT mice recovered on day 7, CB_2R KO mice continued to present significantly more behavioural impairments than sham-operated mice. The lack of recovery over time observed in CB_2R KO mice could be associated with the greater lesion size and more TIM-3/Iba-1 expression in the thalamus and in the whole brain, suggesting that the worse behavioural outcome and slower recovery in CB_2R KO mice is due to the presence of increased inflammatory processes. In the rotarod assessing motor learning, we observed deficits only in lesioned CB_2R KO mice at 24 and 72 h after HI, which did not completely recover on day 7 of testing with respect to sham-operated controls. The differential effect between genotypes is probably explained by the fact that lesioned

WT mice showed little damage to striatal and motor cortical areas with respect to CB_2R KO mice, in agreement with our positive correlation results between the extent of brain injury and deficits in the rotarod. Furthermore, we found a significant association between greater rotarod deficits with higher TIM-3/Iba-1 expression in areas involved in motor learning, such as the motor cortex and dorsal striatum, but also in limbic structures like the nucleus accumbens and amygdala. The striatum has been implicated in various motor tasks including motor skill learning in the rotarod (Dang et al., 2006). Previous results have shown that CB_2R in the striatum are up-regulated in response to a lesion (Sagredo et al., 2009), although they are not abundant in this area. Interestingly, deficits in the beam walking test, evaluating motor coordination and balance were correlated with the extent of lesioned area, and with TIM-3/Iba-1 expression in another limbic structure, the olfactory tubercle. The associations found between TIM-3/Iba-1 expression in limbic brain structures with motor learning, balance and coordination deficits suggest that these tasks are sensitive to inflammatory damage in brain networks related to emotional processing. Together, our findings are consistent with the crucial role played by CB_2R in response to an injury and with their participation in progressive recovery of function.

In the hippocampus, a significant increase in the co-expression of TIM-3/Iba-1 was observed in KO with respect to WT mice, although no differences were observed in the object recognition test in lesioned WT and KO mice, a task that has been shown to be dependent on the integrity of the hippocampus (Yi et al., 2016). Future studies should address the question of the potential beneficial effects of CB_2R agonists for the long-lasting memory alterations produced by inflammatory processes in the hippocampus during stroke and hypoxic conditions.

In summary, we demonstrate for the first time the modulation of the pro-inflammatory factors, HIF-1α and TIM-3 in microglia by CB_2R following brain damage induced by HI in adult mice, which seems to participate in the neuroprotective effects of these receptors. Moreover, our results suggest that CB_2R in microglia under these conditions act as a defensive mechanism to prevent inflammation mediated by HIF-1α and TIM-3, and reduce subsequent behavioural alterations. These findings provide a new mechanism that furthers our understanding of the neuroprotective effects of CB_2R, and suggest new therapeutic avenues to manage the debilitating consequences of brain damage following hypoxic stroke.

References

Anderson, A.C., Anderson, D.E., Bregoli, L., Hastings, W.D., Kassam, N., Lei, C., Chandwaskar, R., Karman, J., Su, E.W., Hirashima, M., Bruce, J.N., Kane, L.P., Kuchroo, V.K., Hafler, D. a, 2007. Promotion of tissue inflammation by the immune receptor Tim-3 expressed on innate immune cells. Science 318, 1141–1143. doi:10.1126/science.1148536

Ashton, J.C., Rahman, R.M.A., Nair, S.M., Sutherland, B.A., Glass, M., Appleton, I., 2007. Cerebral hypoxia-ischemia and middle cerebral artery occlusion induce expression of the cannabinoid CB2 receptor in the brain. Neurosci. Lett. 412, 114–117. doi:10.1016/j.neulet.2006.10.053

Atwood, B.K., Mackie, K., 2010. CB2: a cannabinoid receptor with an identity crisis. Br. J. Pharmacol. 160, 467–79. doi:10.1111/j.1476-5381.2010.00729.x

Blanco-Calvo, E., Rivera, P., Arrabal, S., Vargas, A., Pavón, F.J., Serrano, A., Castilla-Ortega, E., Galeano, P., Rubio, L., Suárez, J., Rodriguez de Fonseca, F., 2014. Pharmacological blockade of either cannabinoid CB1 or CB2 receptors prevents both cocaine-induced conditioned locomotion and cocaine-induced reduction of cell proliferation in the hippocampus of adult male rat. Front. Integr. Neurosci. 7, 106. doi:10.3389/fnint.2013.00106

Buckley, N.E., McCoy, K.L., Mezey, É., Bonner, T., Zimmer, A., Felder, C.C., Glass, M., Zimmer, A., 2000. Immunomodulation by cannabinoids is absent in mice deficient for the cannabinoid CB2 receptor. Eur. J. Pharmacol. 396, 141–149. doi:10.1016/S0014-2999(00)00211-9

Choi, I.Y., Ju, C., Anthony Jalin, A.M.A., Lee, D.I., Prather, P.L., Kim, W.K., 2013. Activation of cannabinoid CB2 receptor-mediated AMPK/CREB pathway reduces cerebral ischemic injury. Am. J. Pathol. 182, 928–939. doi:10.1016/j.ajpath.2012.11.024

Cutando, L., Busquets-Garcia, A., Puighermanal, E., Gomis-González, M., Delgado-García, J.M., Gruart, A., Maldonado, R., Ozaita, A., 2013. Microglial activation underlies cerebellar deficits produced by repeated cannabis exposure. J. Clin. Invest. 123, 2816–31. doi:10.1172/JCI67569

Dang, M.T., Yokoi, F., Yin, H.H., Lovinger, D.M., Wang, Y., Li, Y., 2006. Disrupted motor learning and long-term synaptic plasticity in mice lacking NMDAR1 in the striatum. Proc. Natl. Acad. Sci. U. S. A. 103, 15254–15259. doi:10.1073/pnas.0601758103

de Fonseca, F.R., del Arco, I., Bermudez-Silva, F.J., Bilbao, A., Cippitelli, A., Navarro, M., 2005. The

endocannabinoid system: Physiology and pharmacology. Alcohol Alcohol. 40, 2–14. doi:10.1093/alcalc/agh110

Fernández-Ruiz, J., Pazos, M.R., García-Arencibia, M., Sagredo, O., Ramos, J.A., 2008. Role of CB2 receptors in neuroprotective effects of cannabinoids. Mol. Cell. Endocrinol. 286, S91-6. doi:10.1016/j.mce.2008.01.001

Flynn, R.W. V, MacWalter, R.S.M., Doney, A.S.F., 2008. The cost of cerebral ischaemia. Neuropharmacology 55, 250–256. doi:10.1016/j.neuropharm.2008.05.031

Franco, R., Fernández-Suárez, D., 2015. Alternatively activated microglia and macrophages in the central nervous system. Prog. Neurobiol. 131, 65–86. doi:10.1016/j.pneurobio.2015.05.003

Guo, K., Mou, X., Huang, J., Xiong, N., Li, H., 2014. Trans-Caryophyllene Suppresses Hypoxia-Induced Neuroinflammatory Responses by Inhibiting NF-κB Activation in Microglia. J. Mol. Neurosci. 54, 41–48. doi:10.1007/s12031-014-0243-5

Irwin, S., 1968. Comprehensive observational assessment: Ia. A systematic, quantitative procedure for assessing the behavioral and physiologic state of the mouse. Psychopharmacology (Berl). 13, 222–257.

Kearn, C.J., Hilliard, C.S., 1997. Rat microglial cell express the peripheral-type cannabinoid receptor (CB2) which is negativelly coupled to adenylyl cyclase, in: Proceedings of the Symposium on the Cannabinoids. International Cannabinoid Research Society. Burlington, p. 57.

Koh, H.S., Chang, C.Y., Jeon, S.-B., Yoon, H.J., Ahn, Y.-H., Kim, H.-S., Kim, I.-H., Jeon, S.H., Johnson, R.S., Park, E.J., 2015. The HIF-1/glial TIM-3 axis controls inflammation-associated brain damage under hypoxia. Nat. Commun. 6, 6340. doi:10.1038/ncomms7340

Kwakkel, G., Kollen, B.J., 2013. Predicting activities after stroke: what is clinically relevant? Int. J. Stroke 8, 25–32. doi:10.1111/j.1747-4949.2012.00967.x

Levine, S., 1960. Anoxic-ischemic encephalopathy in rats. Am. J. Pathol. 36, 1–17.

Lopez-Rodriguez, A.B., Siopi, E., Finn, D.P., Marchand-Leroux, C., Garcia-Segura, L.M., Jafarian-Tehrani, M., Viveros, M.-P., 2015. CB1 and CB2 Cannabinoid Receptor Antagonists Prevent Minocycline-Induced Neuroprotection Following Traumatic Brain Injury in Mice. Cereb. Cortex 25, 35–45. doi:10.1093/cercor/bht202

Maresz, K., Carrier, E.J., Ponomarev, E.D., Hillard, C.J., Dittel, B.N., 2005. Modulation of the cannabinoid CB2 receptor in microglial cells in response to inflammatory stimuli. J. Neurochem. 95, 437–445. doi:10.1111/j.1471-4159.2005.03380.x

Mecha, M., Feliú, A., Carrillo-Salinas, F.J., Rueda-Zubiaurre, A., Ortega-Gutiérrez, S., de Sola, R.G., Guaza, C., 2015. Endocannabinoids drive the acquisition of an alternative phenotype in microglia. Brain. Behav. Immun. 49, 233–245. doi:10.1016/j.bbi.2015.06.002

Mechoulam, R., Parker, L. a., 2011. The Endocannabinoid System and the Brain. Annu. Rev. Psychol. 64, 120717165617008. doi:10.1146/annurev-psych-113011-143739

Murikinati, S., Jüttler, E., Keinert, T., Ridder, D. a, Muhammad, S., Waibler, Z., Ledent, C., Zimmer, A., Kalinke, U., Schwaninger, M., 2010. Activation of cannabinoid 2 receptors protects against cerebral ischemia by inhibiting neutrophil recruitment. FASEB J. 24, 788–798. doi:10.1096/fj.09-141275

Olson, E.E., McKeon, R.J., 2004. Characterization of cellular and neurological damage following unilateral hypoxia/ischemia. J. Neurol. Sci. 227, 7–19. doi:10.1016/j.jns.2004.07.021

Paxinos, G., Franklin, K.B.J., 2001. The Mouse Brain in Stereotaxic Coordinates, 2nd editio. ed. Academic Press.

Pazos, M.R., Núñez, E., Benito, C., Tolón, R.M., Romero, J., 2005. Functional neuroanatomy of the endocannabinoid system. Pharmacol. Biochem. Behav. 81, 239–47. doi:10.1016/j.pbb.2005.01.030

Rice, J.E., Vannucci, R.C., Brierley, J.B., 1981. The influence of immaturity on hypoxic-ischemic brain damage in the rat. Ann. Neurol. 9, 131–141. doi:10.1002/ana.410090206

Rivers-Auty, J.R., Smith, P.F., Ashton, J.C., 2014. The cannabinoid CB2 receptor agonist GW405833 does not ameliorate brain damage induced by hypoxia-ischemia in rats. Neurosci. Lett. 569, 104–109. doi:10.1016/j.neulet.2014.03.077

Rousselet, E., Kriz, J., Seidah, N.G., 2012. Mouse model of intraluminal MCAO: cerebral infarct evaluation by cresyl violet staining. J. Vis. Exp. doi:10.3791/4038

Sagredo, O., González, S., Aroyo, I., Pazos, M.R., Benito, C., Lastres-Becker, I., Romero, J.P., Tolón, R.M., Mechoulam, R., Brouillet, E., Romero, J., Fernández-Ruiz, J., 2009. Cannabinoid CB2 receptor agonists protect the striatum against malonate toxicity: relevance for Huntington's disease. Glia 57, 1154–67. doi:10.1002/glia.20838

Schmidt, W., Schäfer, F., Striggow, V., Fröhlich, K., Striggow, F., 2012. Cannabinoid receptor subtypes 1 and 2 mediate long-lasting neuroprotection and improve motor behavior deficits after transient focal cerebral ischemia. Neuroscience 227, 313–26. doi:10.1016/j.neuroscience.2012.09.080

Sheng, H., Laskowitz, D.T., Pearlstein, R.D., Warner, D.S., 1999. Characterization of a recovery global cerebral ischemia model in the mouse. J. Neurosci. Methods 88, 103–109. doi:10.1016/S0165-0270(99)00018-7

Sheng, W.S., Hu, S., Min, X., Cabral, G.A., Lokensgard, J.R., Peterson, P.K., 2005. Synthetic cannabinoid WIN55,212-2 inhibits generation of inflammatory mediators by IL-1beta-stimulated human astrocytes. Glia 49, 211–9. doi:10.1002/glia.20108

Shi, H., 2009. Hypoxia inducible factor 1 as a therapeutic target in ischemic stroke. Curr. Med. Chem. 16, 4593–600.

Shi, Q., Zhang, P., Zhang, J., Chen, X., Lu, H., Tian, Y., Parker, T.L., Liu, Y., 2009. Adenovirus-mediated brain-derived neurotrophic factor expression regulated by hypoxia response element protects brain from injury of transient middle cerebral artery occlusion in mice, Neuroscience Letters. doi:10.1016/j.neulet.2009.08.049

Ternianov, A., Pérez-Ortiz, J.M., Solesio, M.E., García-Gutiérrez, M.S., Ortega-Álvaro, A., Navarrete, F., Leiva, C., Galindo, M.F., Manzanares, J., 2012. Overexpression of CB2 cannabinoid receptors results in neuroprotection against behavioral and neurochemical alterations induced by intracaudate administration of 6-hydroxydopamine. Neurobiol. Aging 33, 421.e1-16. doi:10.1016/j.neurobiolaging.2010.09.012

Van Sickle, M.D., Duncan, M., Kingsley, P.J., Mouihate, A., Urbani, P., Mackie, K., Stella, N., Makriyannis, A., Piomelli, D., Davison, J.S., Marnett, L.J., Di Marzo, V., Pittman, Q.J., Patel, K.D., Sharkey, K. a, 2005. Identification and Functional Characterization of Brainstem Cannabinoid \mathrmCB_2 Receptors. Science (80-.). 310, 329–332. doi:10.1126/science.1115740

Wellons III, J.C., Sheng, H., Laskowitz, D.T., Burkhard Mackensen, G., Pearlstein, R.D., Warner, D.S., 2000. A comparison of strain-related susceptibility in two murine recovery models of global cerebral ischemia. Brain Res. 868, 14–21. doi:10.1016/S0006-8993(00)02216-2

Woodroofe, M.N., Sarna, G.S., Wadhwa, M., Hayes, G.M., Loughlin, A.J., Tinker, A., Cuzner, M.L., 1991.

Detection of interleukin-1 and interleukin-6 in adult rat brain, following mechanical injury, by in vivo microdialysis: evidence of a role for microglia in cytokine production. J. Neuroimmunol. 33, 227–36.

Yi, J.H., Park, H.J., Kim, B.C., Kim, D.H., Ryu, J.H., 2016. Evidences of the role of the rodent hippocampus in the non-spatial recognition memory. Behav. Brain Res. 297, 141–9. doi:10.1016/j.bbr.2015.10.018

Yonekura, I., Kawahara, N., Nakatomi, H., Furuya, K., Kirino, T., 2004. A Model of Global Cerebral Ischemia in C57 BL/6 Mice. J. Cereb. Blood Flow Metab. 24, 151–158. doi:10.1097/01.WCB.0000096063.84070.C1

Zarruk, J.G., Fernández-López, D., García-Yébenes, I., García-Gutiérrez, M.S., Vivancos, J., Nombela, F., Torres, M., Burguete, M.C., Manzanares, J., Lizasoain, I., Moro, M. a, 2012. Cannabinoid type 2 receptor activation downregulates stroke-induced classic and alternative brain macrophage/microglial activation concomitant to neuroprotection. Stroke 43, 211–219. doi:10.1161/STROKEAHA.111.631044

Zhang, M., Adler, M.W., Abood, M.E., Ganea, D., Jallo, J., Tuma, R.F., 2009. CB2 receptor activation attenuates microcirculatory dysfunction during cerebral ischemic/reperfusion injury. Microvasc. Res. 78, 86–94. doi:10.1016/j.mvr.2009.03.005

Zhang, M., Martin, B.R., Adler, M.W., Razdan, R.K., Ganea, D., Tuma, R.F., 2008. Modulation of the balance between cannabinoid CB1 and CB2 receptor activation during cerebral ischemic/reperfusion injury. Neuroscience 152, 753–760. doi:10.1016/j.neuroscience.2008.01.022

Zhang, M., Martin, B.R., Adler, M.W., Razdan, R.K., Jallo, J.I., Tuma, R.F., 2007. Cannabinoid CB(2) receptor activation decreases cerebral infarction in a mouse focal ischemia/reperfusion model. J. Cereb. Blood Flow Metab. 27, 1387–96. doi:10.1038/sj.jcbfm.9600447

FIGURE LEGENDS

Figure 1. Representative coronal brain sections stained with Cresyl violet from WT sham-operated (A), non-lesioned (B) and lesioned (C) mice; and CB_2R KO sham-operated (D), non-lesioned (E) and lesioned (F) mice following HI displaying the extent of the lesioned area in the ipsilateral hemisphere to the carotid ligation (defined in red). The bar graph (G) represents the quantification of lesion extent with respect to the contralateral hemisphere in 13 WT and 26 KO lesioned mice (**p<0.01).

Figure 2. Behavioural performance in WT and CB_2R KO lesioned (L), and non-lesioned (NL) mice following HI, and in sham-operated controls (sham) at 24 h, 72 h and 7 days after HI. (A) Behavioural studies in the Irwin Test, (B) fall latency in the rotarod test, (C) arrival latency in the beam walking test, (D) locomotor activity in the open field test (WT lesioned n=13, non-lesioned n=34, sham-operated n=17; KO lesioned n=26, non-lesioned n=22, sham-operated n=14), and (E) discrimination index in the novel object recognition test (WT lesioned n=7, non-lesioned n=22, sham-operated n=8; KO lesioned n=15, non-lesioned n=16, sham-operated n=7). In A-C: ***p<0.001 vs. 24 h; &&& p<0.001 vs. 72 h; ##p<0.01, ###p<0.001 vs. WT lesioned mice. In E: $$$ p<0.001 (lesion effect).

Figure 3. Quantification of GFAP and Iba-1 immunostaining in WT and KO mice. Expression of GFAP positive cells in the ipsilateral motor cortex (A), the striatum (B), and the hippocampus (C) ***p<0.001 (group effect). Expression of Iba-1-positive cells in the ipsilateral motor cortex (D), the striatum (E), and the hippocampus (E). The data represent mean + S.E.M. cells per mm^2 (percent of contralateral hemisphere) in WT sham-operated (n=7), non-lesioned (n=7), and lesioned (n=7), and in KO sham-operated (n=7), non-lesioned (n=7), and lesioned (n=8) mice. Right panels show representative images of GFAP and Iba-1 immunostaining in the ipsilateral (IL) and contralateral (CL) hemispheres from lesioned WT and CB_2R KO mice subjected to HI. Scale bar = 100 μm. **p<0.01, ***p<0.001 (lesion effect); #p<0.05, ###p<0.001 (genotype effect).

Figure 4. Quantification of HIF-1α immunofluorescence in lesioned brain structures from the total number of WT and KO lesioned mice (7 WT and 9 KO) (A-E), and WT and KO with similar moderate brain damage (7 WT and 7 KO) (F-J) in the ipsilateral entorhinal cortex, amygdala, hippocampus, motor cortex, and striatum. The data indicate the mean + S.E.M. number of positive HIF-1α/Iba-1 cells/mm^2. The left panels are representative photomicrographs of brain sections showing expression of HIF-1α, Iba-1 and merged co-expression (white arrows) in different structures of both genotypes. Scale bar = 50 μm. *p<0.05, **p<0.001.

Figure 5. Quantification of HIF-1α immunofluorescence in non-lesioned brain structures from the total number of WT and KO lesioned mice (7 WT and 9 KO) (A-D), and WT and KO with similar moderate brain damage (7 WT and 7 KO) (E-H) in the ipsilateral olfactory tubercle, nucleus accumbens, septum, and thalamus. The data indicate the mean + S.E.M. number of positive HIF-1α/Iba-1 cells/mm^2. The left panels are representative photomicrographs of brain sections showing expression of HIF-1α, Iba-1 and merged co-expression (white arrows) in different structures of both genotypes. Scale bar = 50 μm. *p<0.05, **p<0.001.

Figure 6. Quantification of TIM-3 immunofluorescence in lesioned brain structures from the total number of lesioned WT (n = 7) and KO (n = 10) mice (A-D), and in WT (n = 7) and KO (n = 7) mice with similar moderate brain damage (D-G) in the ipsilateral sensory cortex, entorhinal cortex, amygdala and hippocampus. The data indicate the mean + S.E.M. number of positive Tim-3/Iba-1 cells/mm^2. The left panels are representative photomicrographs of brain sections showing expression of TIM-3, Iba-1 and merged co-expression (white arrows) in different structures of both genotypes. Scale bar = 50 μm. *p<0.05, **p<0.001.

Figure 7. Quantification of TIM-3 immunofluorescence in lesioned brain structures (KO mice) from the total number of WT (n = 7) and KO (n = 10) mice (A-B), and in WT (n = 7) and KO (n = 7) mice with similar moderate brain damage (C-D) in the ipsilateral motor cortex and striatum. The data indicate the mean + S.E.M. number of positive Tim-3/Iba-1 cells/mm^2. The left panels are representative photomicrographs of

brain sections showing expression of TIM-3, Iba-1 and merged co-expression (white arrows) in different structures of both genotypes. Scale bar = 50 µm. *p<0.05, **p<0.001.

Figure 8. Quantification of TIM-3 immunofluorescence in non-lesioned brain structures from the total number of WT (n = 7) and KO (n = 10) mice (A-D), and in mice with similar moderate brain damage WT (n = 7) and KO (n = 7) (E-H) in the ipsilateral olfactory tubercle, nucleus accumbens, septum, and thalamus. The data indicate the mean + S.E.M. number of positive TIM-3/Iba-1 cells/mm^2. The left panels are representative photomicrographs of brain sections showing expression of TIM-3, Iba-1 and merged co-expression (white arrows) in different structures of both genotypes. Scale bar = 50 µm. *p<0.05, **p<0.001.

Figure 9. Correlation analyses between behavioural deficits with the extent of the lesion, and with TIM-3/Iba-1 immunoreactivity co-expression in different brain areas. (A) Behavioural deficits in the Irwin test were significantly correlated with the extent of the lesion (p<0.001), and with TIM-3/Iba-1 expression in the thalamus (p<0.05) and total brain expression (p<0.05). (B) Rotarod deficits were significantly correlated with the extent of the lesion (p<0.001), and with TIM-3/Iba-1 expression in the motor cortex (p<0.05), total cortex (p<0.01), striatum (p<0.05), nucleus accumbens (p<0.01), and amygdala (p<0.05). (C) Beam walking deficits were significantly correlated with the extent of the lesion (p<0.001), and with TIM-3/Iba-1 expression in the olfactory tubercle (p<0.05).

Supp. Figure 1. Morphological analyses of activated microglial cell types in the ipsilateral motor cortex (A), the striatum (B), and the hippocampus (C) of lesioned WT and KO mice. The data indicate the mean + S.E.M. number of reactive microglial cells of type I, II III, IV and type V. ***p<0.001 (cell type effect).

Supp. Table 1. Experimental sequence describing the number of mice used in each procedure.

CB2 cannabinoid receptors modulate HIF-1α and TIM-3 expression in a hypoxia-ischemia mouse model

Elk Kossatz[1], Rafael Maldonado[1] and Patricia Robledo[1, 2]

[1]Laboratory of Neuropharmacology, Pompeu Fabra University, PRBB, Barcelona, Spain

[2]Integrative Pharmacology and Systems Neuroscience, IMIM-Hospital del Mar Research Institute, PRBB, Barcelona, Spain.

Corresponding Authors:
Patricia Robledo, PhD
Integrative Pharmacology and Systems Neuroscience
IMIM-Hospital del Mar Research Institute
PRBB
Calle Dr. Aiguader 88
Barcelona 08003
SPAIN
probledo@imim.es
rafael.maldonado@upf.edu
Tel: +34 93 316 0455
FAX: +34 93 316 0901

Rafael Maldonado, MD, PhD
Laboratory of Neuropharmacology
Pompeu Fabra University
PRBB
Calle Dr. Aiguader 88
Barcelona 08003
SPAIN
rafael.maldonado@upf.edu
Tel: +34 93 316 0824
FAX: +34 93 316 0901

Total word-count: 7393

ABSTRACT

The role of CB2 cannabinoid receptors (CB_2R) in global brain lesions induced by hypoxia-ischemia (HI) insult is still unresolved. The aim of this study was to evaluate the involvement of CB_2R in the behavioural and biochemical underpinnings related to brain damage induced by HI in adult mice, and the mechanisms involved. CB_2R knockout (KO) mice and wild-type littermates (WT) underwent permanent ligation of the left common carotid artery and hypoxia. Behavioural measurements in the rotarod, beam walking, object recognition, open field, and Irwin tests were carried out 24 h, 72 h and 7 days. In KO mice, more extensive brain injury was observed. Behavioural deficits in the Irwin test were observed in both genotypes; while WT mice showed progressive recovery by day 7, KO mice did not. Only KO mice showed alterations in motor learning, coordination and balance, and did not recover over time. A higher expression of microglia and astrocytes was observed in several brain areas of lesioned WT and KO mice. The possible alteration of the inflammatory-related factors HIF-1α and TIM-3 was evaluated in these animals. In both genotypes, HIF-1α and TIM-3 expression was observed in lesioned areas associated with activated microglia. However, the expression levels of these proteins were exacerbated in KO mice in several lesioned and non-lesioned brain structures. Our results indicate that CB_2R may have a crucial neuroprotective role following HI insult through the modulation of the inflammatory-related HIF-1α/TIM-3 signalling pathway in microglia.

Keywords: Hypoxia-ischemia, inflammation, TIM-3, HIF-1α, microglia, motor learning, cannabinoid receptors

1. Introduction

Cerebral ischemia related with stroke, cardiac arrest, cardiovascular surgery, and neurosurgical procedures is one of the major causes of death and disability world-wide, and represents a great burden to society (Flynn et al., 2008). These conditions are often associated with low blood oxygen content (hypoxia), and lead to a complex cascade of events in the brain including oxidative stress, inflammation and neuronal death (Choi et al., 2013). Brain ischemia often leads to death, but those patients who survive show major neurological deficits depending on the area of the brain affected (Kwakkel and Kollen, 2013). Thus, treatment strategies have been focused on pharmacological agents that can help to accelerate recovery of function. Animal models of hypoxia-ischemia (HI) injury can be useful tools to better understand the mechanisms involved in these conditions, and to design more efficacious therapeutic strategies. In this study, we used a model of HI that was originally described by Levine in 1960 to study perinatal and neonatal hypoxia, applying it to adult mice. **This model of global hypoxia with unilateral ischemia** is relevant in situations in which the brain is deprived of both oxygen content and blood flow, such as cardiac arrest and neurovascular surgeries (Olson and McKeon, 2004). Previous studies using this model in adult mice have shown that HI induces important histopathological and behavioural changes including glial activation, cell death and motor deficits (**Olson and McKeon, 2004; Koh et al., 2014; Ashton et al., 2007; Fernandez-Ruiz et al., 2008 and Zhang et al., 2008).**

The endocannabinoid system has been studied as a possible target for neuroprotective strategies in ischemia-induced brain damage. This system consists of two main receptors, cannabinoid type 1 receptors (CB_1R) and cannabinoid type 2 receptors (CB_2R), their endogenous ligands, mainly N-arachidonoylethanolamine (anandamide) and 2-arachidonoylglycerol (2-AG) and their corresponding synthesizing and degrading enzymes (Mechoulam and Parker, 2011). CB_1R are highly expressed in the central nervous system (CNS), while CB_2R are mainly localized in immune cells such as lymphocytes, neutrophils and microglia/macrophages (de Fonseca et al., 2005; Pazos et al., 2005), but also in brain neurons (Van Sickle et al., 2005).

Importantly, CB_2R appear to be localized in both astrocytes and microglia (Kearn and Hilliard, 1997; Sheng et al., 2005), and their expression is increased in these types of cells in response to inflammatory stimuli during experimental autoimmune encephalomyelitis (Maresz et al., 2005), and following inflammation associated to ischemic and HI episodes (Ashton et al., 2007; Fernández-Ruiz et al., 2008; Zhang et al., 2008). Various studies have evaluated the neuroprotective role of CB_2R activation following brain damage due to cerebral ischemia. Thus, the CB_2R agonist, trans-caryophyllene suppressed hypoxia-induced cytotoxicity of cultured BV_2 microglia cells through inhibition of NF-κB activation (Guo et al., 2014). In addition, administration of the CB_2R agonists, JWH-133 (Murikinati et al., 2010; Zarruk et al., 2012), O-3853 and O-1966 (Zhang et al., 2007) attenuated infarct volume in mice following middle cerebral artery occlusion (MCAO), although, one study shows that the CB_2R agonist GW405833 does not ameliorate brain damage induced by HI in rats (Rivers-Auty et al., 2014). The beneficial effects of CB_2R agonists were attributed to the inhibition by CB_2R of either neutrophil recruitment (Murikinati et al., 2010), inhibition of leukocyte/endothelial adhesion (Zhang et al., 2007), or to a decrease in microglia/macrophage activation (Zarruk et al., 2012). Only a few genetic studies have evaluated the role of CB_2R in focal ischemia with contradictory results (Murikinati et al., 2010; Zarruk et al., 2012; Zhang et al., 2009). Moreover, the mechanisms involved in the neuroprotective role of CB_2R in global brain injury following HI in adult mice are still largely unknown.

Interestingly, recent findings reveal that HI injury in adult mice, increases the expression of the T-cell immunoglobulin and mucin domain protein (TIM-3) in activated microglia, and this effect is mediated by the hypoxia-inducible factor 1 (HIF-1) (Koh et al., 2015). HIF-1 is a heterodimeric transcriptional regulator of various genes under hypoxic conditions, and has been implicated in inflammatory responses after ischemia (Shi, 2009). TIM-3 is expressed in various immune cell types including microglia, where it modulates adaptive and innate immunity, and is a key promoter of tissue inflammation (Anderson et al., 2007). Since the expression of CB_2R increases in activated microglia (Atwood and Mackie, 2010), and CB_2R regulate microglial activation in pathological conditions (Mecha et al., 2015), we tested the hypothesis that CB_2R may confer neuroprotection after HI through modulation of the HIF-1α/TIM-3 axis.

Therefore, we assessed brain damage in adult WT and CB_2R KO mice subject to HI conditions, and determined the associated behavioural alterations at three different time-points (24 h, 72 h and 7 days) post-insult. In addition, we evaluated the expression levels of astrocytes and activated microglia, as well as the levels of the pro-inflammatory factors, HIF-1α and TIM-3 in activated microglia of several brain structures of both genotypes.

2. Experimental Procedures

2.1. Animals

Homozygote male CB_2R KO mice and WT littermates on a C57BL/6J background (kindly provided by Nancy E. Buckley, Cal State Polytechnic University, Pomona, CA) (Buckley et al., 2000), were bred in the animal facilities of the PRBB. Mice (8 to 15 weeks old) were group-housed and maintained in a temperature (21±1 °C) and humidity (65±10%) controlled room with food and water available *ad libitum*. All the experiments were performed during the light phase of the dark/light cycle (lights on from 08:00 to 20:00 h). Animal procedures were conducted in accordance with the standard ethical guidelines (EU Directive 2010/63/EU for animal experiments), and approved by the local ethical committee (CEEA, PRBB). All experiments were performed under blind conditions. **At the end of the experimental procedure, in order to confirm the genotype of the mice, DNA was obtained from the tail. Genotyping was performed routinely by PCR analysis using the following primers: 5'-GGGGATCGATCCGTCCTGTAAGTCT-3' (CB_2KO forward); 5'-GGAGTTCAACCCCATGAAGGAGTAC-3' (WT forward); 5'- GACTAGAGCTTTGTAGGTAGGCGGG -3' (WT and CB_2KO reverse).**

2.2. Surgery

Mice were randomly assigned to either the sham-operated group or the HI groups. The HI procedure was adapted from a previously described methodology (Levine, 1960; Rice et al., 1981). Briefly, mice were anesthetized with isoflurane (mixture of O_2 and N_2O (0.3/0.7 L/min), and placed on a heat plate to maintain a constant body temperature of 37 °C during the surgery. A median incision in the neck was performed exposing the left common carotid artery, which was then isolated from nerve and vein to permanently ligated it in two locations with 4-0 surgical silk. The carotid artery was not severed in order to prevent possible death from haemorrhage. The ligature was placed just proximal to the bifurcation of the common carotid artery into the internal and external carotid artery. The wound was then sutured, and the animals were returned to their cages. Hypoxic episodes were conducted 60 min after left common carotid artery

occlusion, when the animals had recovered from anaesthesia and presented normal behaviours. A hypoxia chamber (BioSpherix, NY, USA) was used to conduct hypoxic episodes consisting of a constant flow of 10% oxygen for 60 min. The temperature of the mice (37 ºC) was maintained inside the chamber via heating devices placed beneath the animal cage. Sham-operated animals received common carotid artery isolation, but no ligation or hypoxia was performed. After the HI episode, mice were allowed free access to food and water. Body temperature was measured before and after surgery, and before and after hypoxia by using a mouse rectal probe. Sixty seven WT and 58 KO mice followed the HI procedure, while 17 WT and 14 KO mice were sham-operated controls.

2.3. Behavioural tests

In order to evaluate the behavioural, motor and cognitive alterations associated with HI, sham-operated and HI mice were tested in the rotarod, the beam-walking, the open field and the Irwin test 24 h, 72 h and 7 days after the procedure. Cognitive performance was tested 72 h and 7 days after HI using the novel object recognition test (NOR). **All of the tests were conducted by observers blind to the experimental conditions.**

Irwin test. Mice were placed in a Plexiglas cylinder and a modified Irwin test (Irwin, 1968) was conducted to evaluate subjective signs of behavioural dysfunction produced by HI and the sham operation. Several symptoms were evaluated by their presence or absence (loss of balance, ptosis and loss of traction) on a 1 point scale. Other symptoms were rated on a 2-point scale (abnormal gait, piloerection, low reactivity to touch), and neurological deficits rated on a scale from 0-2 (no deficit = 0, forelimb weakness and torso turning to the affected side when held by de tail = 1, or circling to affected side = 2). The final score was expressed by the sum of all symptoms observed in each animal (Total from 0 to11).

Open field test. Mice were placed in an experimental arena (Plexiglas box, 90x70) in order to evaluate locomotor activity, and the total distance travelled was determined by counting the number of squares crossed (units) during a 5 min period.

Rotarod test. The accelerating rotarod (Panlab) was used to evaluate motor coordination. Mice were trained for 2 days before HI. Each training day consisted of 60 sec at 6 rpm (day 1) and 60 sec at 8 rpm (day 2). The test day consisted of 5 trials using the rotarod in acceleration mode from 4 rpm to 20 rpm until the animal fell from the rod. The latency to fall off the rod on every trial was determined, and the mean of the 5 trials was used in the data analysis.

Beam-walking test. To evaluate motor coordination and balance, the beam-walking test was performed. This test examines the ability of the animal to remain upright and to walk on an elevated beam with varying thicknesses. The beams consisted of 1-m long strips of wood with 20 or 6 mm square cross sections. The beams were placed horizontally, 40 cm above the floor, with one end mounted on a support and the other end attached to the home cage of the animal as the escape box. Mice were trained for 2 days before HI. Each training day consisted in the animal traversing the 20 mm square beam (2 trials) and on the test day, mice traversed a narrower beam of 6 mm. The latency to traverse the beam was determined, and the analysis was based on the mean scores of the two trials.

Novel object recognition test (NOR). In this paradigm, a black Plexiglas maze with two corridors (30 cm long x 4.5 cm wide, and 15 cm high walls) set at a 90° angle (Panlab) was used. First, mice were habituated to the empty maze for 9 min. Twenty-four h later, mice were place back in the maze for another 9 min, but this time two identical objects were presented, one on each arm of the maze, and the time that the mice spent exploring each object was recorded. The mice were again placed in the maze 3 h later for 9 min, but one of the familiar objects was replaced with a novel object, and the total time spent exploring each object (novel and familiar) was recorded. Object exploration was defined as the orientation of the nose to the object at a distance of less than 2 cm. A discrimination index was calculated as the time spent exploring the novel object minus the time exploring the familiar object divided by the total time exploring both objects. A higher discrimination index is considered to reflect greater memory retention.

2.4. Histological analysis

The extent of the lesion was visualized using a standard Cresyl violet staining protocol. With this procedure the infarct area can be identified by the loss of Nissl staining in the HI ipsilateral

hemisphere. One group of mice (see Supp. Table 1) were euthanized by cervical dislocation, and fresh brains were harvested and sliced at 20 µm with a cryostat and mounted onto gelatin-coated slides and stored at -80 °C. Brain slices were divided into 5 parallel series from 1.98 to 1.34 , from 1.18 to 0.38, from -0.22 to -0.88, from -1.46 to -2.06 and from -2.30 to -2.96 relative to Bregma (Paxinos and Franklin, 2001). The stained sections of the brain were analysed at 1x (zoom factor 0.8x) using an Olympus MVX10 Macro Zoom Microscope equipped with Olympus DP71 digital camera. The ischemic lesion was delimited using the ImageJ software. For each mouse, the lesioned area was calculated in 5 brain sections, and the sum in pixels was transformed to μm^2 and expressed as a percentage of the contralateral hemisphere in order to correct for possible oedema in the ipsilateral hemisphere (Rousselet et al., 2012).

To determine the expression levels of glial fibrillary acid protein (GFAP) and Iba-1 in different brain areas, we performed immunohistochemistry in a different group of mice (see Supp. Table 1). Mice were deeply anesthetized by intraperitoneal injection (0.2 ml per 10 g body weight) of a mixture of ketamine (100 mg per kg) and xylazine (20 mg per kg), and intracardially perfused with 4% paraformaldehyde in 0.1 M phosphate buffer (pH 7.5), delivered with a peristaltic pump. Brains were post-fixed overnight at 4 °C in the same fixative solution and cryoprotected in a solution of 30% sucrose at 4ºC during 24 h. Brain sections were sliced at 30 µm with a microtome and stored at 4ºC in a solution containing 5% sucrose and 0.02% sodium azide in 0.1 M phosphate buffer. Free floating coronal sections from 1.18 to 0.38 and from -1.46 to -2.06 relative to Bregma were collected to determine the expression of glial fibrillary acid protein (GFAP) and Iba-1 in motor cortex, striatum and hippocampus. **In addition, brain sections were stained with Cresyl violet to determine the extent of lesions in these mice.** The immunohistochemical procedure was adapted from a previously described methodology (Blanco-Calvo et al., 2014). Briefly, the sections were placed in a blocking solution containing 10% normal goat serum, 0.3% triton X-100, and 0.1% sodium azide in PBS for 1 h, incubated overnight in the following diluted primary antibodies at 4°C: rabbit anti-GFAP (1:500, Dako; cat. #Z0334) or rabbit anti-Iba1 (1:500, Wako; cat. no. 019-19741). On day two, sections were incubated with biotinylated goat anti-rabbit IgG (1:500, Vector; cat. no.BA-1000), and ExtrAvidin peroxidase (Sigma, cat. no. E2886) diluted 1:2000 at room temperature for 1 h. Immunolabeling was revealed with 0.05% DAB (Sigma), 0.05% nickel ammonium

sulphate, and 0.03% H_2O_2 in PBS. Sections were mounted and analysed at 20x using a Leica DMR microscope equipped with a digital camera Leica DFC 300FX. Three images per structure were analysed in order to quantify manually GFAP and Iba-1 cells expression using ImageJ software (NIH). The mean number of cells per mm^2 was plotted for motor cortex, striatum and hippocampus in WT and KO mice.

To determine the expression levels of TIM-3, HIF-1α and Iba-1 in different structures of the brain, immunofluorescence studies were carried out as previously described (Cutando et al., 2013). Free-floating slices were placed in 0.3% Triton X-100, 10% donkey serum (Sigma) in PB, and incubated overnight at 4°C with the following primary antibodies: anti- HIF-1α (1: 200, Abcam; cat. no. ab16066), anti-Iba-1 (1:500, Wako; cat. no. 019-19741) and anti-TIM-3 (1:500, R&D systems, cat. no. AF1529). The following day, sections were incubated for 2 h at room temperature with Alexa 647 donkey anti-mouse-IR, Alexa 488 donkey anti–rabbit-Cy2 and Alexa 555 donkey anti-goat-Cy3 (1:500; Invitrogen/ Molecular Probes), and mounted. Confocal images were obtained using a Leica TSC SP8 confocal microscope at 20X with a 1.5 zoom increase. Eighteen images of stained sections (from Bregma +1.18 mm to Bregma –2.30 mm) were analysed using ImageJ software (NIH) in order to manually quantify the expression of Iba-1/TIM-3, and Iba-1/HIF-1α. Positive cells in each structure were averaged and compared between genotypes.

2.5. Morphological analysis of activated microglia

To assess whether the reactive microglia observed following HI in WT and KO mice presented differential morphologies, we analysed the Iba-1 immunostained sections using the methodology previously reported (Lopez-Rodriguez et al., 2015). Cells were classified according to five types: Type I, cells with two or less cellular processes; Type II, cells showing 3 to 5 short branches; Type III, cells with more than 5 and longer processes and small cell bodies; Type IV, cells with large somas and retracted, thicker processes; Type V, cells with amoeboid cell bodies and many short processes. Reactive microglia (Types III, IV and V) cells were counted in the hippocampus, the striatum and the motor cortex of WT and KO lesioned mice by visual inspection of the images obtained from stained sections showing Iba-1 positive cells. We then

grouped cell types I, II, III and IV that correspond to an M2 (anti-inflammatory) phenotype, and cell type V to an M1 (pro-inflammatory) phenotype (Franco and Fernández-Suárez, 2015).

2.6. Statistical analyses

The behavioural data were analysed using repeated measures ANOVA with time (24 h, 72 h and 7 days) as within subjects factor, genotype (CB_2R KO and WT mice), and lesion (lesioned, non-lesioned) as between subject factors, followed by the Fisher's LSD *post-hoc* test for multiple comparisons when appropriate. The mortality and variability (lesion vs. non-lesion) ratios were evaluated with the χ-square non-parametrical test. The extent of the lesion was analysed **using the Student's t-test**. The immunohistochemistry data and the morphological characteristics of microglial cells were analysed using a two-way ANOVA with genotype and lesion or genotype and cell type as between subject factors followed by a Fisher's LSD *post-hoc* when appropriate. The immunofluorescence results were analysed between genotypes using one-way ANOVA. Correlations between TIM-3/Iba-1 expression and behavioural outcomes were analysed using the Spearman correlation test. All data were expressed as the mean + S.E.M. A p-value below 0.05 was considered statistically significant. The statistical analyses were performed with the "Statistica" programme, version 6 (StatSoft Inc.), except for correlations, where the GraphPad Prism software was used (GraphPad Software).

3. Results

3.1. Mortality and severity of the lesion in WT and CB_2R KO mice following HI

Twenty out of 67 WT and 10 out of 58 CB_2R KO mice did not survive following the HI procedure. Most deaths in WT and KO mice occurred on the day of the surgery during the hypoxia procedure and it was not possible to extract the brains in time to visualize any differences between genotype in the extent of the brain lesion. Among those mice that survived the HI procedure, there were 3 KO mice that died 1, 3 and 5 days following HI, and 2 WT mice that died 1 and 2 days after HI. Although a higher percentage of WT than KO mice died (30% in WT vs. 17% in KO mice), no significant differences in mortality ratio were observed between genotypes. Two different types of animals survived: those that exhibited lesions in the

ipsilateral hemisphere to the carotid ligation, and those that did not show overt lesions. In WT, 13 out of 47 mice were lesioned, and 34 out of 47 mice showed no apparent infarct. In KO animals, 26 out of 48 mice were lesioned, while 22 out of 48 mice were not lesioned. Thus, a greater percentage of CB_2R KO mice showed lesions as compared to WT mice (54% in KO vs. 28% in WT mice; $p < 0.01$, χ^2 test).

HI-induced brain damage ipsilateral to the carotid ligation was observed in WT mice in hippocampal areas CA1, CA2 and CA3, and in the sensory, entorhinal and piriform cortices (Fig. 1C). In CB_2R KO mice, more extensive brain injury was observed including the hippocampus, sensory, entorhinal, piriform and motor cortices, the dorsal striatum, the Globus pallidus and the amygdala (Fig. 1F). Accordingly, CB_2R KO mice showed higher overall brain damage than WT mice (27 % in KO vs. 12 % in WT mice; **p<0.01**) (Figure 1G). The contralateral hemisphere remained intact in both genotypes. In sham and HI non-lesioned mice of both genotypes, no overt signs of brain injury were observed in either hemisphere (Fig. 1).

3.2. CB_2R KO mice show greater behavioural, motor coordination and balance deficits than WT mice following HI

To assess behavioural, motor coordination, and balance deficits we used the Irwin, the rotarod, the open field, and the beam walking tests. Six groups of mice were included in these studies: three groups of WT mice (13 lesioned, 34 non-lesioned and 17 sham-operated), and three groups of KO mice (26 lesioned, 22 non-lesioned and 14 sham-operated).

Qualitative symptoms of behavioural dysfunction were evaluated 24 h, 72 h and 7 days following HI using the Irwin test (Fig. 2A). Repeated measures ANOVA revealed a significant main effect of time of testing ($F(2,202)=35.1$, $p<0.001$), and lesion ($F(2,101)=25.4$, $p<0.001$), **but no significant main effect of genotype.** Significant interactions were observed between time and genotype ($F(2,202)= 7.4$, **p<0.001**), and time and lesion ($F(4,202)=11.7$, $p<0.001$). Post-hoc analysis 24 h after HI showed a significant increase in symptoms in WT lesioned ($p<0.001$) and non-lesioned ($p<0.05$) mice with respect to sham-operated WT animals, and in KO lesioned mice with respect to sham-operated KO mice ($p<0.001$). At 72 h, both WT and KO mice showed signs of dysfunction with respect to their respective control groups ($p<0.05$). At 7 days post-insult, only KO lesioned mice showed deficits with respect to controls ($p<0.05$).

These data indicate that WT mice progressively recover functionality, while KO mice show persistent symptoms of behavioural dysfunction even 7 days after HI insult.

In the rotarod test, deficits were observed 24 h, 72 h and 7 days following HI (Fig. 2B). Repeated measures ANOVA revealed a significant effect of time ($F(2,218)=21.1$. $p<0.001$), genotype ($F(1,109)=15.9$, $p<0.001$), and interaction between genotype and lesion ($F(2,109)=8.4$, $p<0.001$), and between time and **genotype** ($F(2,218)=6.0$, $p<0.01$). **Post-hoc analysis at 72 h and 7 days showed a significant decrease in fall latency in KO mice with respect to sham-operated controls ($p<0.05$), and with respect to WT lesioned mice ($p<0.001$).** No significant deficits in performance were observed at any time point in WT lesioned mice or in non-lesioned mice of either genotype.

In the beam walking test, deficits were observed in KO mice at 24 h, 72 h and 7 days following HI (Fig. 2C). Repeated measures ANOVA revealed a significant effect of time ($F(2,214)=28.1$, $p<0.001$), genotype ($F(1,107)=4.6$, $p<0.05$), lesion ($F(2,107)=6.0$, $p<0.01$), and interactions between genotype and lesion ($F(2,107)=6.2$, **$p<0.01$**), time and lesion ($F(4,214)=5.2$, $p<0.001$), and between time, genotype and lesion ($F(4,214)=2.4$, $p<0.05$). Post-hoc analysis 24 h after HI showed a significant increase in arrival latency in KO ($p<0.001$) with respect to sham-operated KO mice ($p<0.001$), and lesioned WT mice ($p<0.01$). At 72 h, KO lesioned mice showed a significant increase in arrival latency with respect to sham-operated controls ($p<0.05$). At 7 days following HI, KO lesioned mice still showed some non-significant deficits with respect to sham-operated control mice. No significant deficits were observed at any time point in WT lesioned mice or in non-lesioned mice of either genotype.

In the open field test, both WT and KO lesioned mice showed slight non-significant decreases in locomotor activity 24 h following HI, which recovered at 72 h and 7 days post-insult (Fig. 2D).

In the NOR test (WT: 7 lesioned, 22 non-lesioned and 8 sham-operated; KO: 15 lesioned, 16 non-lesioned and 7 sham-operated) mice were evaluated. Robust memory deficits were observed 72 h and 7 days following HI in both WT and KO lesioned mice (Fig. 2E). Repeated measures ANOVA revealed a significant main effect of lesion ($F(2,61)=38.7$, $p<0.001$), indicating that lesioned mice of both genotypes

showed deficits in recognition memory with respect to sham-operated controls, but no significant differences were observed between genotypes or time of testing.

3.3. Increased glial expression in the cortex, striatum and hippocampus of WT and CB_2R KO mice following HI

The analysis of GFAP and Iba-1 positive cells was carried out in 7 WT and 8 KO lesioned, 7 WT and 7 KO non-lesioned, and 7 WT and 7 KO sham-operated mice. Following HI, GFAP expression was increased in the ipsilateral hemisphere of WT and KO mice with respect to the contralateral hemisphere in the motor cortex (Fig. 3A), striatum (Fig. 3B) and hippocampus (Fig. 3C). In the motor cortex, statistical analysis revealed a significant effect of lesion ($F(2,35)=15.1$, $p<0.001$), but no significant effect of genotype or interaction between factors. Similarly, in the striatum a significant effect of lesion ($F(2,32)=12.0$, $p<0.001$), but no significant effect of genotype or interaction between factors were observed. Finally, in the hippocampus, statistical analysis revealed a significant effect of lesion ($F(2,31)=55.9$, $p<0.001$), but no significant effect of genotype or interaction between factors.

Iba-1 expression was increased in ipsilateral lesioned areas of the motor cortex (Fig.3D), striatum (Fig 3E) and hippocampus (Fig. 3F) of WT and KO mice compared to the contralateral hemisphere following HI. In the motor cortex, a significant effect of genotype ($F(1,33)=4.8$, $p<0.05$), lesion ($F(2,33)=6.3$, $p<0.01$), but no significant interaction between factors were observed. Similarly, in the striatum, a significant effect of lesion ($F(2,35)=26.8$, $p<0.001$), but no significant effect of genotype or interaction between factors were revealed. In the hippocampus however, a significant effect of genotype ($F(1,34)=5.6$, $p<0.05$), lesion ($F(2,34)=111.9$, $p<0.001$), and interaction between factors ($F(2,34)=6.6$, $p<0.01$) were found. The post-hoc test showed a significant increase in Iba-1 expression in WT ($p<0.001$) and KO ($p<0.001$) lesioned mice with respect to sham-operated animals. In addition, KO lesioned mice showed higher Iba-1 expression than WT lesioned mice ($p<0.001$).

To analyse the morphology of the activated microglia observed in lesioned WT (n=7) and CB_2R KO (n=8) mice, we classified these cells into morphological types I, II III and IV (M2, anti-inflammatory), or type V (M1, pro-inflammatory) phenotype (Supp. Fig. 1). The results showed a similar number of pro- and anti-

inflammatory associated phenotype in the hippocampus in both WT and KO mice. Statistical analysis revealed a significant effect of cell type in the motor cortex ($F(1,13)= 195.8$, $p<0.001$) and in the striatum ($F(1,13)=44.8$, $p<0.001$), indicating more anti-inflammatory than pro-inflammatory cells in both genotypes.

3.4. Increased HIF-1α expression in microglia of WT and CB_2R KO mice following HI

To evaluate the HIF-1α expression in microglia in different brain structures following HI, we performed double immunofluorescence studies (Iba-1 and HIF-1α) in brain sections of WT and CB_2R KO mice, and two different analyses were performed. **One analysis including the total size group of WT and KO lesioned mice (7 WT: mean ± S.E.M. lesion size = 9 ± 1.76%, and 9 KO: mean ± S.E.M. lesion size = 27% ± 7.03; $p<0.05$) (Fig. 4 A-E and 5 A-D), and another analysis considering only similar moderate lesion size sub-groups (7 WT: mean ± S.E.M. lesion size = 9% ± 1.76, and 7 KO mean ± S.E.M. lesion size = 14% ± 1.75; n.s.) (Fig. 4 F-J and 5 E-H). The criteria used to consider a moderate lesion was less than 27% of lesioned area with respect to the contralateral hemisphere.**

In the total size group analysis, higher expression levels of HIF-1α in microglia were observed in lesioned areas of KO with respect to WT mice in the ipsilateral entorhinal cortex ($F(1,9)=6.6$, $p<0.05$) (Fig. 4A), amygdala ($F1,10)=5.1$, $p<0.05$) (Fig. 4B), hippocampus ($F(1,10)= 11.5$, $p<0.01$) (Fig. 4C), motor cortex ($F(1,12)=13.4$, $p<0.01$) (Fig. 4D), and striatum ($F(1,13)=9.6$, $p<0.01$) (Fig. 4E) In non-lesioned areas, higher expression levels in KO with respect to WT mice were found in olfactory tubercle ($F(1,11)= 8.0$, $p<0.05$) (Fig. 5A), nucleus accumbens ($F(1,12)=12.2$, $p<0.01$) (Fig. 5B), lateral septum ($F(1,10)= 7.1$, $p<0.05$) (Fig. 5C) and thalamus ($F(1,11)=6.4$, $p<0.05$) (Fig. 5D).

In the similar moderate lesion size sub-groups, higher expression levels of HIF-1α in microglia were observed in lesioned areas of KO with respect to WT mice in the ipsilateral entorhinal cortex ($F(1,8)=7.2$, $p<0.05$) (Fig. 4F), hippocampus ($F(1,8)=6.1$, $p<0.05$) (Fig. 4H), motor cortex ($F(1,10)=8.3$, $p<0.05$) (Fig. 4I), and striatum ($F(1,11)=9.0$, $p<0.05$) (Fig. 4J). In non-lesioned areas, higher expression levels in KO with respect to WT mice were found in olfactory tubercle ($F(1,10)= 6.9$, $p<0.05$) (Fig. 5E), nucleus accumbens ($F(1,10)=8.8$, $p<0.05$) (Fig. 5F) and lateral septum ($F(1,8)= 9.9$, $p<0.05$) (Fig. 5G).

3.5. Increased TIM-3 expression in microglia of WT and CB_2R KO mice following HI

To determine the expression of TIM-3 in microglia in different brain structures following HI, we performed double immunofluorescence studies (Iba-1 and TIM-3) in brain sections of WT and CB_2R KO mice. Two different analyses were performed as described before. **The analysis including the total size group of WT and KO lesioned mice was carried out in 7 WT and 10 KO mice (Figs. 6 A-D , 7 A-B and 8 A-D), and the analysis including similar moderate lesion size sub-groups was performed in 7 WT and 7 KO mice (Figs. 6 E-H , 7 C-D and 8 E-H).**

In the total size group analysis, higher expression levels of TIM-3 in microglia were revealed in lesioned areas of KO with respect to WT mice in the ipsilateral sensory cortex ($F(1,14)=31.7$, $p<0.001$) (Fig. 6A), entorhinal cortex ($F(1,13)=18.4$, $p<0.001$) (Fig. 6B), amygdala ($F1,12)=4.9$, $p<0.05$) (Fig. 6C), hippocampus ($F(1,13)= 8.5$, $p<0.05$) (Fig. 6D), motor cortex ($F(1,14)=5.0$, $p<0.05$) (Fig. 7A) and striatum ($F(1,15)=7.0$, $p<0.05$) (Fig. 7B). In non-lesioned areas, higher expression levels in KO with respect to WT mice were revealed in the olfactory tubercle ($F(1,14)= 4.7$, $p<0.05$) (Fig. 8A) and lateral septum ($F(1,15)= 6.4$, $p<0.05$) (Fig. 8C). No significant effects of genotype were observed in nucleus accumbens or thalamus (Fig. 8 B, D).

In the similar moderate lesion size sub-groups, higher expression levels of TIM-3 in microglia were observed in lesioned areas of KO with respect to WT mice in the ipsilateral sensory cortex ($F(1,12)=8.1$, $p<0.05$) (Fig. 6E), and entorhinal cortex ($F(1,11)=19.1$, $p<0.01$) (Fig. 6F), amygdala ($F1,9)=6.0$, $p<0.05$) (Fig. 6G) and hippocampus ($F(1,11)=5.6$, $p<0.05$) (Fig. 6H). In non-lesioned areas higher expression levels in KO with respect to WT mice were observed in the lateral septum ($F(1,12)= 9.5$, $p<0.01$) (Fig. 8G). No significant effects of genotype were observed in motor cortex, striatum, olfactory tubercle, nucleus accumbens or thalamus (Figs. 7C, D and 8E, F, H).

3.6. Correlations between behavioural output and extent of the lesions and TIM-3/Iba-1 expression levels

Since brain injury and inflammation following HI was observed in several areas of the brain, we tested the hypothesis that particular behavioural alterations would be related to the extent of the lesion and to inflammatory processes in specific brain structures. Thus, we performed correlation analyses in WT and KO mice between behavioural alterations 7 days after the HI insult and the extent of the lesions, and TIM-3/Iba-1 expression levels in different brain structures (Fig. 9). Behavioural deficits in the Irwin test (symptoms) were positively correlated with greater brain damage ($R= 0.51$, $p<0.001$), and with higher TIM-3/Iba-1 co-expression in the thalamus ($R= 0.66$, $p<0.05$), and the overall brain ($R= 0.51$, $p<0.05$) (Fig. 9A). Behavioural deficits in the rotarod test (decreased fall latency) were significantly correlated with greater brain damage ($R= -0.55$, $p<0.001$), and with higher TIM-3/Iba-1 co-expression in the motor cortex ($R=-0.63$, $p<0.05$), overall cortical areas ($R=-0.73$, $p<0.01$), striatum ($R=-0.58$, $p<0.05$), nucleus accumbens ($R=-0.66$, $p<0.01$), and amygdala ($R=-0.60$, $p<0.05$) (Fig. 9B). Alterations in the beam walking test (increased arrival latency) were significantly correlated with greater brain damage ($R= 0.54$, $p<0.001$), and with higher TIM-3/Iba-1 co-expression in the olfactory tubercle ($R= 0.53$, $p<0.05$) (Fig. 9C). No significant correlations were observed in the hippocampus or the lateral septum with any of the behavioural deficits exhibited by WT and KO mice after HI.

4. Discussion

CB_2R KO mice exhibited more extensive brain lesions than WT mice following HI insult, attaining most of the ipsilateral cortex and hippocampus, and even reaching parts of the striatum and amygdala. Accordingly, CB_2R KO mice showed persistent behavioural alterations and deficits in motor learning, coordination and balance. Cognitive performance was severely impaired in both genotypes, and no recovery was observed over time. A significantly higher expression of microglia was observed in the hippocampus of lesioned CB_2R KO with respect to WT mice. TIM-3 expression in microglia was also more extensive in CB_2R KO than in WT mice, and was detected in more medial non-lesioned areas such as the thalamus, olfactory tubercle, nucleus accumbens and septum. **Likewise, HIF-1α expression was also higher in lesioned areas of CB_2R KO compared to WT mice, including the hippocampus, amygdala, motor and entorhinal cortices and striatum, but also in several non-lesioned structures such as the olfactory tubercle, the nucleus accumbens, septum and thalamus.**

Finally, TIM-3/Iba-1 expression in several brain structures significantly correlated with behavioural, motor learning, coordination and balance deficits. These results indicate that CB_2R may modulate inflammatory factors such as TIM-3 following brain damage due to HI insult, and consequently prevent associated behavioural, motor learning, coordination and balance deficits.

To investigate the involvement of CB_2R in global brain injury following HI, we used a new genetic model using CB_2R KO and WT adult mice subjected to a permanent unilateral common carotid artery occlusion followed by hypoxic conditions. Following this procedure, HI produced moderate mortality and variable brain damage, as previously reported (Olson and McKeon, 2004). Although mortality was higher in WT than CB_2R KO mice, no significant differences were found between genotypes. Nonetheless, we cannot rule out that more WT mice died due to more extensive lesions than KO mice. However, this is unlikely since most WT and KO mice died during the HI procedure. In mice that survived, two populations could be observed with regards to brain lesion characteristics: mice exhibiting neuronal damage in the ipsilateral hemisphere, and mice exhibiting no overt lesions in any of the two hemispheres. This fact may be due to individual differences in posterior communicating arteries that form part of the circle of Willis in mice, which

have been shown to affect lesion volume in multiple models of cerebral ischemia (Sheng et al., 1999; Wellons III et al., 2000; Yonekura et al., 2004). The percentage of animals with lesions was significantly higher in the CB_2R KO (54 %) than in the WT (28 %) group, which could be due to a disparate cerebral vascularisation in both genotypes. However, there is no data to support this hypothesis. In addition, there are no studies thoroughly assessing the nature or extent of brain damage occurring in mice lacking CB_2R following HI-induced brain injury. In this study, WT lesioned mice displayed restricted neuronal damage mainly in the hippocampus, with some animals also showing lesions in the sensory, entorhinal or piriform cortices. These results confirm previous evidence regarding the susceptibility of these mouse brain areas to be injured after HI (Olson and McKeon, 2004). On the other hand, CB_2R KO mice showed a larger infarct area at the level of the hippocampus, sensory, entorhinal and piriform cortices, and in addition, damage tissue also comprised the motor cortex, striatum and amygdala. These findings suggest that CB_2R play a general protective role in adult mice subject to HI by preventing a more widespread lesion in the brain.

To examine the behavioural consequences of HI, we determined a general behavioural score in the Irwin test, as well as motor and cognitive performance in WT and CB_2R KO mice 24 h, 72 h and 7 days following this procedure. Behavioural deficits were observed in both genotypes 24 h after HI. However, whereas WT mice recovered over time, CB_2R KO mice did not, indicating that CB_2R are involved in the restoration of function following HI insults. Motor skill learning, coordination and balance were selectively impaired in CB_2KO mice, and no recovery was observed over time. These effects were not due to impaired locomotor activity since distance travelled in the open field was only slightly affected in all the experimental groups. Previous studies have reported neuroprotective effects of CB_2R activation in other animal models. Thus, the administration of a dual CB1/CB2 receptor agonist, KN38-7271 in rats (Schmidt et al., 2012), or the selective CB_2R agonist, O-1966 in mice (Zhang et al., 2009) reduces motor learning impairments induced after MCAO, and the overexpression of CB_2R confers neuroprotection against 6-OHDA-induced lesions of the mouse striatum (Ternianov et al., 2012).

Cognitive function was evaluated using the object recognition test 3 and 7 days following HI. Both WT and CB_2R KO lesioned mice showed severe memory impairments on both testing days. Contrary to the other

behaviours studied, the cognitive deficit found in WT mice was not enhanced in CB_2KO mice, probably due to a ceiling effect that prevented further deficits to be observed in these mice. These results are consistent with the extensive damage induced by HI to the hippocampus in both genotypes, and reveal that even unilateral lesions of this structure are sufficient to profoundly affect cognitive function in mice subjected to these adverse conditions.

We found that the expression of reactive astrocytes was greater in the ipsilateral motor cortex, the striatum and hippocampus of WT and CB_2R KO mice subjected to HI with respect to sham-operated controls. Astrocytes are thought to promote brain repair following traumatic brain injury and stroke conditions, and are up-regulated under HI conditions in the ipsilateral cerebral cortex of mice (Koh et al., 2015; Olson and McKeon, 2004). Furthermore, microglia was also increased in the ipsilateral motor cortex, the striatum of WT and CB_2R KO mice following HI with respect to sham-operated controls. In the hippocampus however, CB_2R KO mice showed higher expression levels than WT mice. **Microglia, which are the main resident immune cells in the brain, are up-regulated following HI episodes (Koh et al., 2015; Olson and McKeon, 2004).** They produce inflammatory mediators (Woodroofe et al., 1991) that contribute to cell death and increased infarct size. Nonetheless, it has been demonstrated that microglia can adopt an alternative phenotype changing from the classical pro-inflammatory M1 to an M2 anti-inflammatory phenotype (Franco and Fernández-Suárez, 2015). Moreover, CB_2R have been implicated in the transformation of microglia to a more protective phenotype (Mecha et al., 2015). Thus, we carried out morphological analyses of microglial cells in WT and KO mice to determine genotype differences in microglial phenotype. This evaluation showed that in areas where brain injury was extensive such as the hippocampus, no differences in the number of cell types I, II, III and IV (anti-inflammatory phenotype), and cell type V (pro-inflammatory phenotype) were observed in either genotype. In contrast, in areas where brain damage was sparse such as the motor cortex and the striatum, more type I, II, III and IV than type V morphologies were found in both WT and KO mice. These findings agree with the dual role (pro- and anti-inflammatory) of microglia following HI conditions (Franco and Fernández-Suárez, 2015) by showing that in salvageable tissue the protective microglial phenotype is more abundant. However, CB_2R do not seem involved in this differential effect of microglia cells.

In order to determine the possible mechanisms involved in these responses of CB_2R, **we evaluated in WT and KO mice the expression of the pro-inflammatory factor HIF-1α in activated microglia,** which is rapidly increased in the cell nucleus following systemic hypoxia, and may contribute to tissue damage (Shi et al., 2009). Because HIF-1α appears mostly to be induced following ischemia in the penumbral tissue, we examined both lesioned and non-lesioned structures in WT and KO mice. We found that HIF-1α expression was higher in lesioned areas of CB_2R KO compared to WT mice, including the hippocampus, amygdala, motor and entorhinal cortices and striatum, but also in several non-lesioned structures such as the olfactory tubercle, the nucleus accumbens, septum and thalamus. These findings suggest that CB_2R may be limiting the detrimental action of HIF-1α under HI to prevent brain damage. Similarly, we also found that the co-expression of TIM-3 and Iba-1 immunofluorescence was exacerbated in CB_2R KO with respect to WT mice in lesioned areas (hippocampus, amygdala, motor and entorhinal cortices and striatum), but also in non-damaged areas (olfactory tubercle and lateral septum). These findings are consistent with recent evidence associating the HIF-1/glial TIM-3 axis with inflammation and brain damage to the cerebral cortex following HI insults (Koh et al., 2015). Our data indicate that the inflammatory process, which results from brain injury after HI is more important in mice lacking CB_2R, covering more medial areas. Importantly, the increase in HIF-1α and TIM-3 in KO mice with respect to WT mice was also observed when we compared animals with similar lesions, especially in entorhinal cortex, hippocampus and septum. These results suggest that HIF-1α and TIM-3 expression is not a consequence of a more extensive lesion size in KO mice, but it is probably due to the lack of CB_2R. Moreover, these findings demonstrate for the first time the role of these receptors in the modulation of the pro-inflammatory factors, HIF-1α and TIM-3, which may underlie this neuroprotective role of CB_2R. Previous reports have shown that pharmacological activation of CB_2R reduces brain damage in the MCAO ischemia model by inhibiting neutrophil recruitment (Murikinati et al., 2010) or by decreasing microglia/macrophage activation (Zarruk et al., 2012). These data, together with recent evidence showing that blockade of TIM-3 reduces neutrophil recruitment by glial cells, and diminishes IL-1β and CXCL1 (Koh et al., 2015), supports our hypothesis that CB_2R play a crucial role in modulating the HIF-1α/TIM-3 axis in microglia to prevent widespread inflammation and global brain damage following HI insults.

Behavioural alterations were significantly associated with greater brain damage and increased expression of TIM-3 in microglia. In the Irwin test, behavioural deficits were observed at 24 and 72 h following HI in both WT and CB_2R KO lesioned mice. However, while WT mice recovered on day 7, CB_2R KO mice continued to present significantly more behavioural impairments than sham-operated mice. The lack of recovery over time observed in CB_2R KO mice could be associated with the greater lesion size and more TIM-3/Iba-1 expression in the thalamus and in the whole brain, suggesting that the worse behavioural outcome and slower recovery in CB_2R KO mice is due to the presence of increased inflammatory processes. In the rotarod assessing motor learning, we observed deficits only in lesioned CB_2R KO mice at 24 and 72 h after HI, which did not completely recover on day 7 of testing with respect to sham-operated controls. The differential effect between genotypes is probably explained by the fact that lesioned WT mice showed little damage to striatal and motor cortical areas with respect to CB_2R KO mice, in agreement with our positive correlation results between the extent of brain injury and deficits in the rotarod. Furthermore, we found a significant association between greater rotarod deficits with higher TIM-3/Iba-1 expression in areas involved in motor learning, such as the motor cortex and dorsal striatum, but also in limbic structures like the nucleus accumbens and amygdala. The striatum has been implicated in various motor tasks including motor skill learning in the rotarod (Dang et al., 2006). Previous results have shown that CB_2R in the striatum are up-regulated in response to a lesion (Sagredo et al., 2009), although they are not abundant in this area. Interestingly, deficits in the beam walking test, evaluating motor coordination and balance were correlated with the extent of lesioned area, and with TIM-3/Iba-1 expression in another limbic structure, the olfactory tubercle. The associations found between TIM-3/Iba-1 expression in limbic brain structures with motor learning, balance and coordination deficits suggest that these tasks are sensitive to inflammatory damage in brain networks related to emotional processing. Together, our findings are consistent with the crucial role played by CB_2R in response to an injury and with their participation in progressive recovery of function.

In the hippocampus, a significant increase in the co-expression of TIM-3/Iba-1 was observed in KO with respect to WT mice, although no differences were observed in the object recognition test in lesioned WT and KO mice, a task that has been shown to be dependent on the integrity of the hippocampus (Yi et al.,

2016). Future studies should address the question of the potential beneficial effects of CB_2R agonists for the long-lasting memory alterations produced by inflammatory processes in the hippocampus during stroke and hypoxic conditions.

In summary, we demonstrate for the first time the modulation of the pro-inflammatory factors, HIF-1α and TIM-3 in microglia by CB_2R following brain damage induced by HI in adult mice, which seems to participate in the neuroprotective effects of these receptors. Moreover, our results suggest that CB_2R in microglia under these conditions act as a defensive mechanism to prevent inflammation mediated by HIF-1α and TIM-3, and reduce subsequent behavioural alterations. These findings provide a new mechanism that furthers our understanding of the neuroprotective effects of CB_2R, and suggest new therapeutic avenues to manage the debilitating consequences of brain damage following hypoxic stroke.

References

Anderson, A.C., Anderson, D.E., Bregoli, L., Hastings, W.D., Kassam, N., Lei, C., Chandwaskar, R., Karman, J., Su, E.W., Hirashima, M., Bruce, J.N., Kane, L.P., Kuchroo, V.K., Hafler, D. a, 2007. Promotion of tissue inflammation by the immune receptor Tim-3 expressed on innate immune cells. Science 318, 1141–1143. doi:10.1126/science.1148536

Ashton, J.C., Rahman, R.M.A., Nair, S.M., Sutherland, B.A., Glass, M., Appleton, I., 2007. Cerebral hypoxia-ischemia and middle cerebral artery occlusion induce expression of the cannabinoid CB2 receptor in the brain. Neurosci. Lett. 412, 114–117. doi:10.1016/j.neulet.2006.10.053

Atwood, B.K., Mackie, K., 2010. CB2: a cannabinoid receptor with an identity crisis. Br. J. Pharmacol. 160, 467–79. doi:10.1111/j.1476-5381.2010.00729.x

Blanco-Calvo, E., Rivera, P., Arrabal, S., Vargas, A., Pavón, F.J., Serrano, A., Castilla-Ortega, E., Galeano, P., Rubio, L., Suárez, J., Rodriguez de Fonseca, F., 2014. Pharmacological blockade of either cannabinoid CB1 or CB2 receptors prevents both cocaine-induced conditioned locomotion and cocaine-induced reduction of cell proliferation in the hippocampus of adult male rat. Front. Integr. Neurosci. 7, 106. doi:10.3389/fnint.2013.00106

Buckley, N.E., McCoy, K.L., Mezey, É., Bonner, T., Zimmer, A., Felder, C.C., Glass, M., Zimmer, A., 2000. Immunomodulation by cannabinoids is absent in mice deficient for the cannabinoid CB2 receptor. Eur. J. Pharmacol. 396, 141–149. doi:10.1016/S0014-2999(00)00211-9

Choi, I.Y., Ju, C., Anthony Jalin, A.M.A., Lee, D.I., Prather, P.L., Kim, W.K., 2013. Activation of cannabinoid CB2 receptor-mediated AMPK/CREB pathway reduces cerebral ischemic injury. Am. J. Pathol. 182, 928–939. doi:10.1016/j.ajpath.2012.11.024

Cutando, L., Busquets-Garcia, A., Puighermanal, E., Gomis-González, M., Delgado-García, J.M., Gruart, A., Maldonado, R., Ozaita, A., 2013. Microglial activation underlies cerebellar deficits produced by repeated cannabis exposure. J. Clin. Invest. 123, 2816–31. doi:10.1172/JCI67569

Dang, M.T., Yokoi, F., Yin, H.H., Lovinger, D.M., Wang, Y., Li, Y., 2006. Disrupted motor learning and long-term synaptic plasticity in mice lacking NMDAR1 in the striatum. Proc. Natl. Acad. Sci. U. S. A. 103, 15254–15259. doi:10.1073/pnas.0601758103

de Fonseca, F.R., del Arco, I., Bermudez-Silva, F.J., Bilbao, A., Cippitelli, A., Navarro, M., 2005. The

endocannabinoid system: Physiology and pharmacology. Alcohol Alcohol. 40, 2–14. doi:10.1093/alcalc/agh110

Fernández-Ruiz, J., Pazos, M.R., García-Arencibia, M., Sagredo, O., Ramos, J.A., 2008. Role of CB2 receptors in neuroprotective effects of cannabinoids. Mol. Cell. Endocrinol. 286, S91-6. doi:10.1016/j.mce.2008.01.001

Flynn, R.W. V, MacWalter, R.S.M., Doney, A.S.F., 2008. The cost of cerebral ischaemia. Neuropharmacology 55, 250–256. doi:10.1016/j.neuropharm.2008.05.031

Franco, R., Fernández-Suárez, D., 2015. Alternatively activated microglia and macrophages in the central nervous system. Prog. Neurobiol. 131, 65–86. doi:10.1016/j.pneurobio.2015.05.003

Guo, K., Mou, X., Huang, J., Xiong, N., Li, H., 2014. Trans-Caryophyllene Suppresses Hypoxia-Induced Neuroinflammatory Responses by Inhibiting NF-κB Activation in Microglia. J. Mol. Neurosci. 54, 41–48. doi:10.1007/s12031-014-0243-5

Irwin, S., 1968. Comprehensive observational assessment: Ia. A systematic, quantitative procedure for assessing the behavioral and physiologic state of the mouse. Psychopharmacology (Berl). 13, 222–257.

Kearn, C.J., Hilliard, C.S., 1997. Rat microglial cell express the peripheral-type cannabinoid receptor (CB2) which is negativelly coupled to adenylyl cyclase, in: Proceedings of the Symposium on the Cannabinoids. International Cannabinoid Research Society. Burlington, p. 57.

Koh, H.S., Chang, C.Y., Jeon, S.-B., Yoon, H.J., Ahn, Y.-H., Kim, H.-S., Kim, I.-H., Jeon, S.H., Johnson, R.S., Park, E.J., 2015. The HIF-1/glial TIM-3 axis controls inflammation-associated brain damage under hypoxia. Nat. Commun. 6, 6340. doi:10.1038/ncomms7340

Kwakkel, G., Kollen, B.J., 2013. Predicting activities after stroke: what is clinically relevant? Int. J. Stroke 8, 25–32. doi:10.1111/j.1747-4949.2012.00967.x

Levine, S., 1960. Anoxic-ischemic encephalopathy in rats. Am. J. Pathol. 36, 1–17.

Lopez-Rodriguez, A.B., Siopi, E., Finn, D.P., Marchand-Leroux, C., Garcia-Segura, L.M., Jafarian-Tehrani, M., Viveros, M.-P., 2015. CB1 and CB2 Cannabinoid Receptor Antagonists Prevent Minocycline-Induced Neuroprotection Following Traumatic Brain Injury in Mice. Cereb. Cortex 25, 35–45. doi:10.1093/cercor/bht202

Maresz, K., Carrier, E.J., Ponomarev, E.D., Hillard, C.J., Dittel, B.N., 2005. Modulation of the cannabinoid CB2 receptor in microglial cells in response to inflammatory stimuli. J. Neurochem. 95, 437–445. doi:10.1111/j.1471-4159.2005.03380.x

Mecha, M., Feliú, A., Carrillo-Salinas, F.J., Rueda-Zubiaurre, A., Ortega-Gutiérrez, S., de Sola, R.G., Guaza, C., 2015. Endocannabinoids drive the acquisition of an alternative phenotype in microglia. Brain. Behav. Immun. 49, 233–245. doi:10.1016/j.bbi.2015.06.002

Mechoulam, R., Parker, L. a., 2011. The Endocannabinoid System and the Brain. Annu. Rev. Psychol. 64, 120717165617008. doi:10.1146/annurev-psych-113011-143739

Murikinati, S., Jüttler, E., Keinert, T., Ridder, D. a, Muhammad, S., Waibler, Z., Ledent, C., Zimmer, A., Kalinke, U., Schwaninger, M., 2010. Activation of cannabinoid 2 receptors protects against cerebral ischemia by inhibiting neutrophil recruitment. FASEB J. 24, 788–798. doi:10.1096/fj.09-141275

Olson, E.E., McKeon, R.J., 2004. Characterization of cellular and neurological damage following unilateral hypoxia/ischemia. J. Neurol. Sci. 227, 7–19. doi:10.1016/j.jns.2004.07.021

Paxinos, G., Franklin, K.B.J., 2001. The Mouse Brain in Stereotaxic Coordinates, 2nd editio. ed. Academic Press.

Pazos, M.R., Núñez, E., Benito, C., Tolón, R.M., Romero, J., 2005. Functional neuroanatomy of the endocannabinoid system. Pharmacol. Biochem. Behav. 81, 239–47. doi:10.1016/j.pbb.2005.01.030

Rice, J.E., Vannucci, R.C., Brierley, J.B., 1981. The influence of immaturity on hypoxic-ischemic brain damage in the rat. Ann. Neurol. 9, 131–141. doi:10.1002/ana.410090206

Rivers-Auty, J.R., Smith, P.F., Ashton, J.C., 2014. The cannabinoid CB2 receptor agonist GW405833 does not ameliorate brain damage induced by hypoxia-ischemia in rats. Neurosci. Lett. 569, 104–109. doi:10.1016/j.neulet.2014.03.077

Rousselet, E., Kriz, J., Seidah, N.G., 2012. Mouse model of intraluminal MCAO: cerebral infarct evaluation by cresyl violet staining. J. Vis. Exp. doi:10.3791/4038

Sagredo, O., González, S., Aroyo, I., Pazos, M.R., Benito, C., Lastres-Becker, I., Romero, J.P., Tolón, R.M., Mechoulam, R., Brouillet, E., Romero, J., Fernández-Ruiz, J., 2009. Cannabinoid CB2 receptor agonists protect the striatum against malonate toxicity: relevance for Huntington's disease. Glia 57, 1154–67. doi:10.1002/glia.20838

Schmidt, W., Schäfer, F., Striggow, V., Fröhlich, K., Striggow, F., 2012. Cannabinoid receptor subtypes 1 and 2 mediate long-lasting neuroprotection and improve motor behavior deficits after transient focal cerebral ischemia. Neuroscience 227, 313–26. doi:10.1016/j.neuroscience.2012.09.080

Sheng, H., Laskowitz, D.T., Pearlstein, R.D., Warner, D.S., 1999. Characterization of a recovery global cerebral ischemia model in the mouse. J. Neurosci. Methods 88, 103–109. doi:10.1016/S0165-0270(99)00018-7

Sheng, W.S., Hu, S., Min, X., Cabral, G.A., Lokensgard, J.R., Peterson, P.K., 2005. Synthetic cannabinoid WIN55,212-2 inhibits generation of inflammatory mediators by IL-1beta-stimulated human astrocytes. Glia 49, 211–9. doi:10.1002/glia.20108

Shi, H., 2009. Hypoxia inducible factor 1 as a therapeutic target in ischemic stroke. Curr. Med. Chem. 16, 4593–600.

Shi, Q., Zhang, P., Zhang, J., Chen, X., Lu, H., Tian, Y., Parker, T.L., Liu, Y., 2009. Adenovirus-mediated brain-derived neurotrophic factor expression regulated by hypoxia response element protects brain from injury of transient middle cerebral artery occlusion in mice, Neuroscience Letters. doi:10.1016/j.neulet.2009.08.049

Ternianov, A., Pérez-Ortiz, J.M., Solesio, M.E., García-Gutiérrez, M.S., Ortega-Álvaro, A., Navarrete, F., Leiva, C., Galindo, M.F., Manzanares, J., 2012. Overexpression of CB2 cannabinoid receptors results in neuroprotection against behavioral and neurochemical alterations induced by intracaudate administration of 6-hydroxydopamine. Neurobiol. Aging 33, 421.e1-16. doi:10.1016/j.neurobiolaging.2010.09.012

Van Sickle, M.D., Duncan, M., Kingsley, P.J., Mouihate, A., Urbani, P., Mackie, K., Stella, N., Makriyannis, A., Piomelli, D., Davison, J.S., Marnett, L.J., Di Marzo, V., Pittman, Q.J., Patel, K.D., Sharkey, K. a, 2005. Identification and Functional Characterization of Brainstem Cannabinoid \mathrmCB_2 Receptors. Science (80-.). 310, 329–332. doi:10.1126/science.1115740

Wellons III, J.C., Sheng, H., Laskowitz, D.T., Burkhard Mackensen, G., Pearlstein, R.D., Warner, D.S., 2000. A comparison of strain-related susceptibility in two murine recovery models of global cerebral ischemia. Brain Res. 868, 14–21. doi:10.1016/S0006-8993(00)02216-2

Woodroofe, M.N., Sarna, G.S., Wadhwa, M., Hayes, G.M., Loughlin, A.J., Tinker, A., Cuzner, M.L., 1991.

Detection of interleukin-1 and interleukin-6 in adult rat brain, following mechanical injury, by in vivo microdialysis: evidence of a role for microglia in cytokine production. J. Neuroimmunol. 33, 227–36.

Yi, J.H., Park, H.J., Kim, B.C., Kim, D.H., Ryu, J.H., 2016. Evidences of the role of the rodent hippocampus in the non-spatial recognition memory. Behav. Brain Res. 297, 141–9. doi:10.1016/j.bbr.2015.10.018

Yonekura, I., Kawahara, N., Nakatomi, H., Furuya, K., Kirino, T., 2004. A Model of Global Cerebral Ischemia in C57 BL/6 Mice. J. Cereb. Blood Flow Metab. 24, 151–158. doi:10.1097/01.WCB.0000096063.84070.C1

Zarruk, J.G., Fernández-López, D., García-Yébenes, I., García-Gutiérrez, M.S., Vivancos, J., Nombela, F., Torres, M., Burguete, M.C., Manzanares, J., Lizasoain, I., Moro, M. a, 2012. Cannabinoid type 2 receptor activation downregulates stroke-induced classic and alternative brain macrophage/microglial activation concomitant to neuroprotection. Stroke 43, 211–219. doi:10.1161/STROKEAHA.111.631044

Zhang, M., Adler, M.W., Abood, M.E., Ganea, D., Jallo, J., Tuma, R.F., 2009. CB2 receptor activation attenuates microcirculatory dysfunction during cerebral ischemic/reperfusion injury. Microvasc. Res. 78, 86–94. doi:10.1016/j.mvr.2009.03.005

Zhang, M., Martin, B.R., Adler, M.W., Razdan, R.K., Ganea, D., Tuma, R.F., 2008. Modulation of the balance between cannabinoid CB1 and CB2 receptor activation during cerebral ischemic/reperfusion injury. Neuroscience 152, 753–760. doi:10.1016/j.neuroscience.2008.01.022

Zhang, M., Martin, B.R., Adler, M.W., Razdan, R.K., Jallo, J.I., Tuma, R.F., 2007. Cannabinoid CB(2) receptor activation decreases cerebral infarction in a mouse focal ischemia/reperfusion model. J. Cereb. Blood Flow Metab. 27, 1387–96. doi:10.1038/sj.jcbfm.9600447

FIGURE LEGENDS

Figure 1. Representative coronal brain sections stained with Cresyl violet from WT sham-operated (A), non-lesioned (B) and lesioned (C) mice; and CB_2R KO sham-operated (D), non-lesioned (E) and lesioned (F) mice following HI displaying the extent of the lesioned area in the ipsilateral hemisphere to the carotid ligation (defined in red). The bar graph (G) represents the quantification of lesion extent with respect to the contralateral hemisphere in **13 WT and 26 KO lesioned mice (**p<0.01)**.

Figure 2. Behavioural performance in WT and CB_2R KO lesioned (L), and non-lesioned (NL) mice following HI, and in sham-operated controls (sham) at 24 h, 72 h and 7 days after HI. (A) Behavioural studies in the Irwin Test, (B) fall latency in the rotarod test, (C) arrival latency in the beam walking test, (D) locomotor activity in the open field test (WT lesioned n=13, non-lesioned n=34, sham-operated n=17; KO lesioned n=26, non-lesioned n=22, sham-operated n=14), and (E) discrimination index in the novel object recognition test (WT lesioned n=7, non-lesioned n=22, sham-operated n=8; KO lesioned n=15, non-lesioned n=16, sham-operated n=7). In A-C: *****p<0.001 vs. 24 h; &&& p<0.001 vs. 72 h; ##p<0.01, ###p<0.001 vs. WT lesioned mice. In E: $$$ p<0.001 (lesion effect).**

Figure 3. Quantification of GFAP and Iba-1 immunostaining in WT and KO mice. Expression of GFAP positive cells in the ipsilateral motor cortex (A), the striatum (B), and the hippocampus (C) ***p<0.001 (group effect). Expression of Iba-1-positive cells in the ipsilateral motor cortex (D), the striatum (E), and the hippocampus (E). The data represent mean + S.E.M. cells per mm^2 (percent of contralateral hemisphere) in WT sham-operated (n=7), non-lesioned (n=7), and lesioned (n=7), and in KO sham-operated (n=7), non-lesioned (n=7), and lesioned (n=8) mice. Right panels show representative images of GFAP and Iba-1 immunostaining in the ipsilateral (IL) and contralateral (CL) hemispheres from lesioned WT and CB_2R KO mice subjected to HI. Scale bar = 100 μm. ****p<0.01, ***p<0.001 (lesion effect); #p<0.05, ###p<0.001 (genotype effect).**

Figure 4. Quantification of HIF-1α immunofluorescence in lesioned brain structures from the total number of WT and KO lesioned mice (7 WT and 9 KO) (A-E), and WT and KO with similar moderate brain damage (7 WT and 7 KO) (F-J) in the ipsilateral entorhinal cortex, amygdala, hippocampus, motor cortex, and striatum. The data indicate the mean + S.E.M. number of positive HIF-1α/Iba-1 cells/mm^2. The left panels are representative photomicrographs of brain sections showing expression of HIF-1α, Iba-1 and merged co-expression (white arrows) in different structures of both genotypes. Scale bar = 50 μm. *p<0.05, **p<0.001.

Figure 5. Quantification of HIF-1α immunofluorescence in non-lesioned brain structures from the total number of WT and KO lesioned mice (7 WT and 9 KO) (A-D), and WT and KO with similar moderate brain damage (7 WT and 7 KO) (E-H) in the ipsilateral olfactory tubercle, nucleus accumbens, septum, and thalamus. The data indicate the mean + S.E.M. number of positive HIF-1α/Iba-1 cells/mm^2. The left panels are representative photomicrographs of brain sections showing expression of HIF-1α, Iba-1 and merged co-expression (white arrows) in different structures of both genotypes. Scale bar = 50 μm. *p<0.05, **p<0.001.

Figure 6. Quantification of TIM-3 immunofluorescence in lesioned brain structures from the total number of lesioned WT (n = 7) and KO (n = 10) mice (A-D), and in WT (n = 7) and KO (n = 7) mice with similar moderate brain damage (D-G) in the ipsilateral sensory cortex, entorhinal cortex, amygdala and hippocampus. The data indicate the mean + S.E.M. number of positive Tim-3/Iba-1 cells/mm^2. The left panels are representative photomicrographs of brain sections showing expression of TIM-3, Iba-1 and merged co-expression (white arrows) in different structures of both genotypes. Scale bar = 50 μm. *p<0.05, **p<0.001.

Figure 7. Quantification of TIM-3 immunofluorescence in lesioned brain structures (KO mice) from the total number of WT (n = 7) and KO (n = 10) mice (A-B), and in WT (n = 7) and KO (n = 7) mice with similar moderate brain damage (C-D) in the ipsilateral motor cortex and striatum. The data indicate the mean + S.E.M. number of positive Tim-3/Iba-1 cells/mm^2. The left panels are representative photomicrographs of

brain sections showing expression of TIM-3, Iba-1 and merged co-expression (white arrows) in different structures of both genotypes. Scale bar = 50 µm. *p<0.05, **p<0.001.

Figure 8. Quantification of TIM-3 immunofluorescence in non-lesioned brain structures from the total number of WT (n = 7) and KO (n = 10) mice (A-D), and in mice with similar moderate brain damage WT (n = 7) and KO (n = 7) (E-H) in the ipsilateral olfactory tubercle, nucleus accumbens, septum, and thalamus. The data indicate the mean + S.E.M. number of positive TIM-3/Iba-1 cells/mm^2. The left panels are representative photomicrographs of brain sections showing expression of TIM-3, Iba-1 and merged co-expression (white arrows) in different structures of both genotypes. Scale bar = 50 µm. *p<0.05, **p<0.001.

Figure 9. Correlation analyses between behavioural deficits with the extent of the lesion, and with TIM-3/Iba-1 immunoreactivity co-expression in different brain areas. (A) Behavioural deficits in the Irwin test were significantly correlated with the extent of the lesion (p<0.001), and with TIM-3/Iba-1 expression in the thalamus (p<0.05) and total brain expression (p<0.05). (B) Rotarod deficits were significantly correlated with the extent of the lesion (p<0.001), and with TIM-3/Iba-1 expression in the motor cortex (p<0.05), total cortex (p<0.01), striatum (p<0.05), nucleus accumbens (p<0.01), and amygdala (p<0.05). (C) Beam walking deficits were significantly correlated with the extent of the lesion (p<0.001), and with TIM-3/Iba-1 expression in the olfactory tubercle (p<0.05).

Supp. Figure 1. Morphological analyses of activated microglial cell types in the ipsilateral motor cortex (A), the striatum (B), and the hippocampus (C) of lesioned WT and KO mice. The data indicate the mean + S.E.M. number of reactive microglial cells of type I, II III, IV and type V. ***p<0.001 (cell type effect).

Supp. Table 1. Experimental sequence describing the number of mice used in each procedure.

Figure 1

Click here to download high resolution image

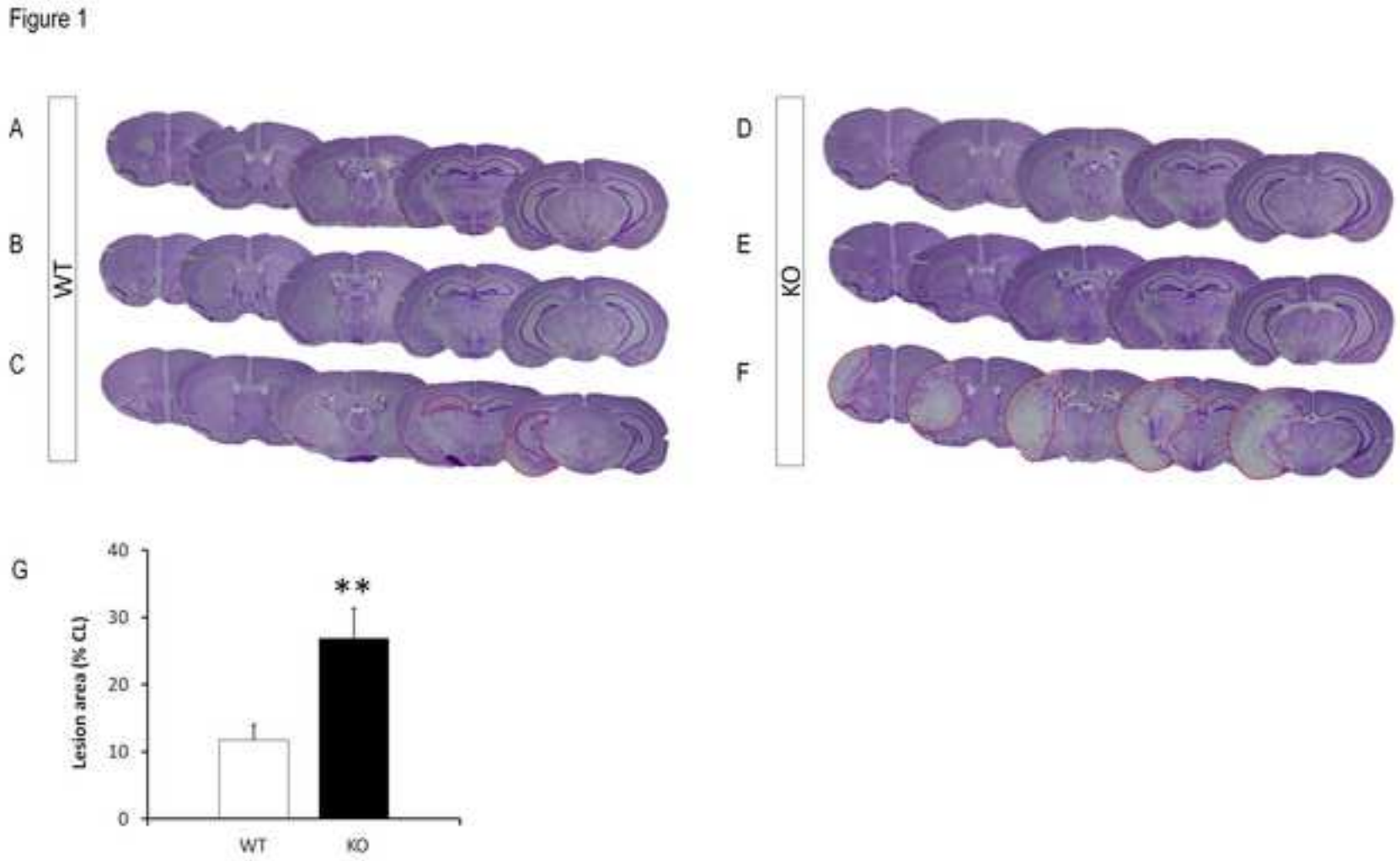

Figure 2

Click here to download high resolution image

Figure 2

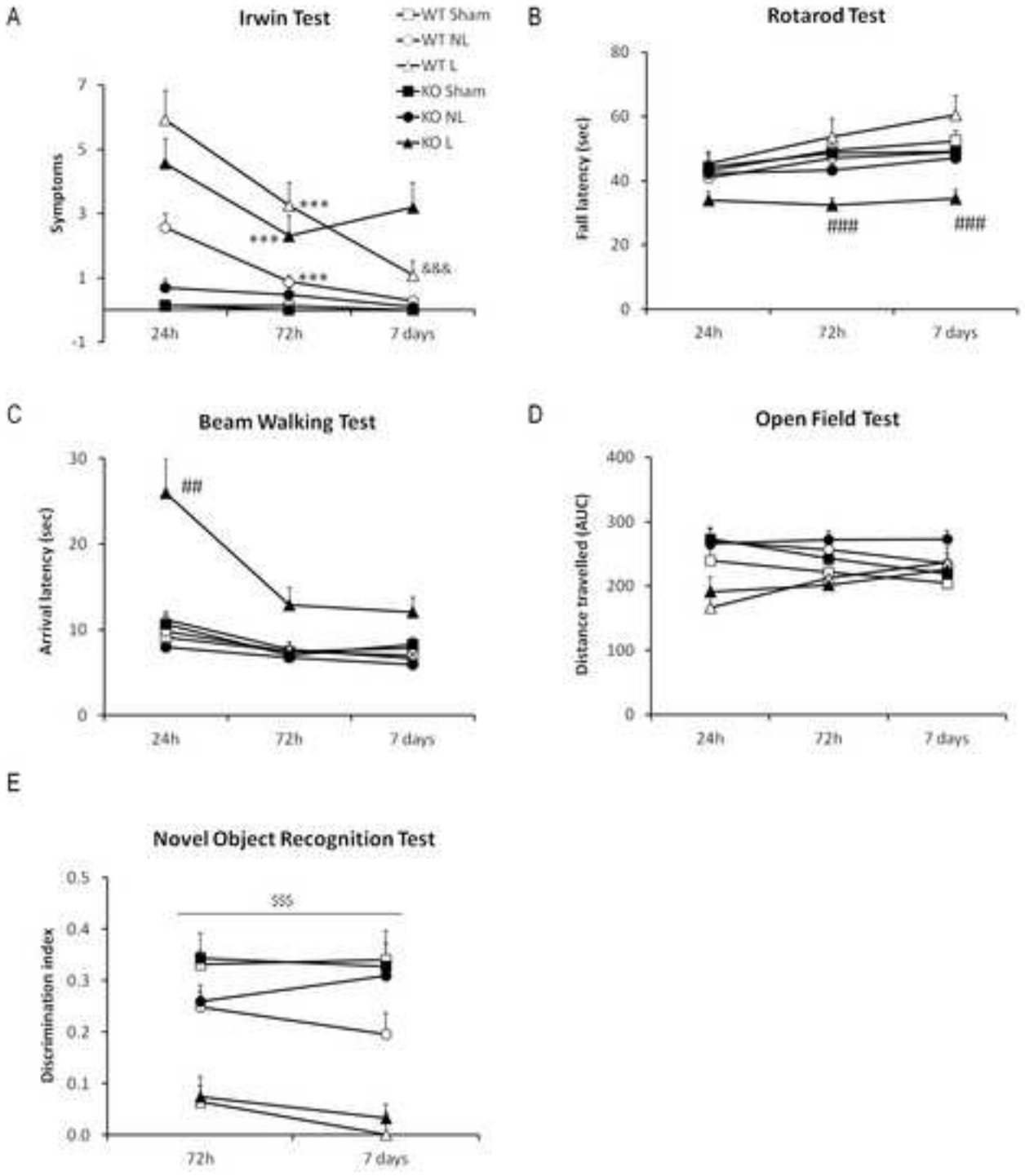

Figure 3

Click here to download high resolution image

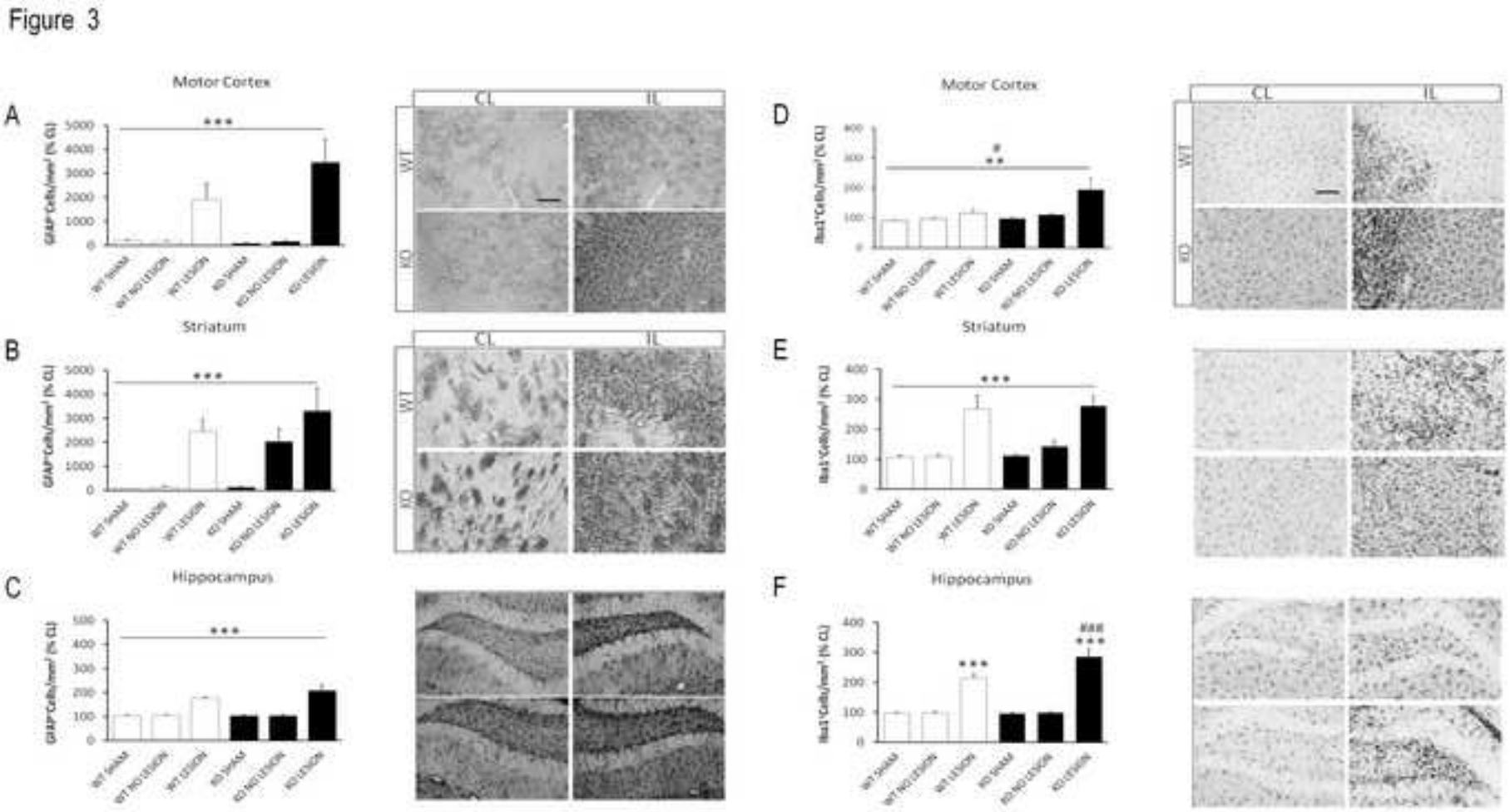

Figure 4

Click here to download high resolution image

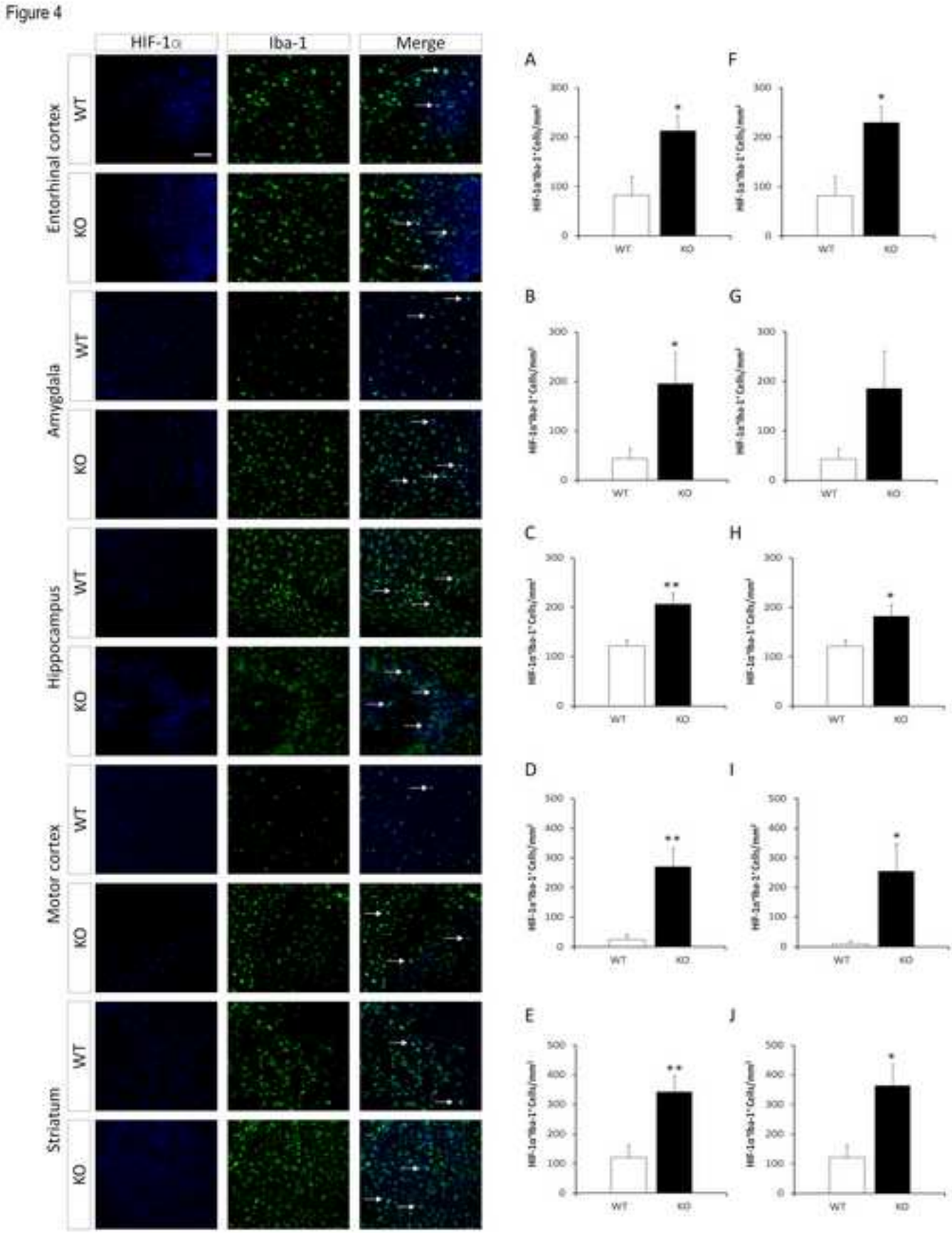

Figure 5

Click here to download high resolution image

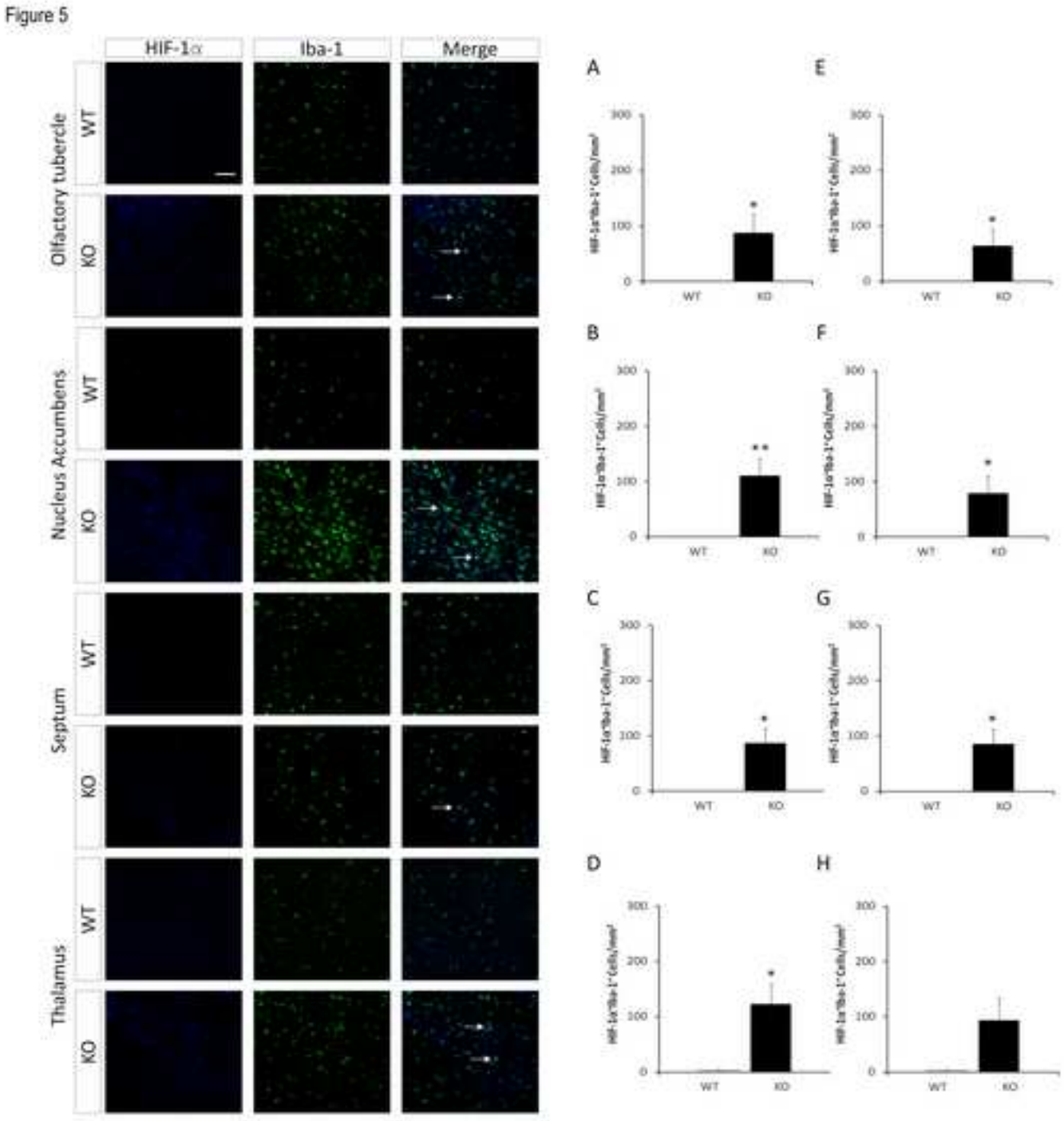

Figure 6

Click here to download high resolution image

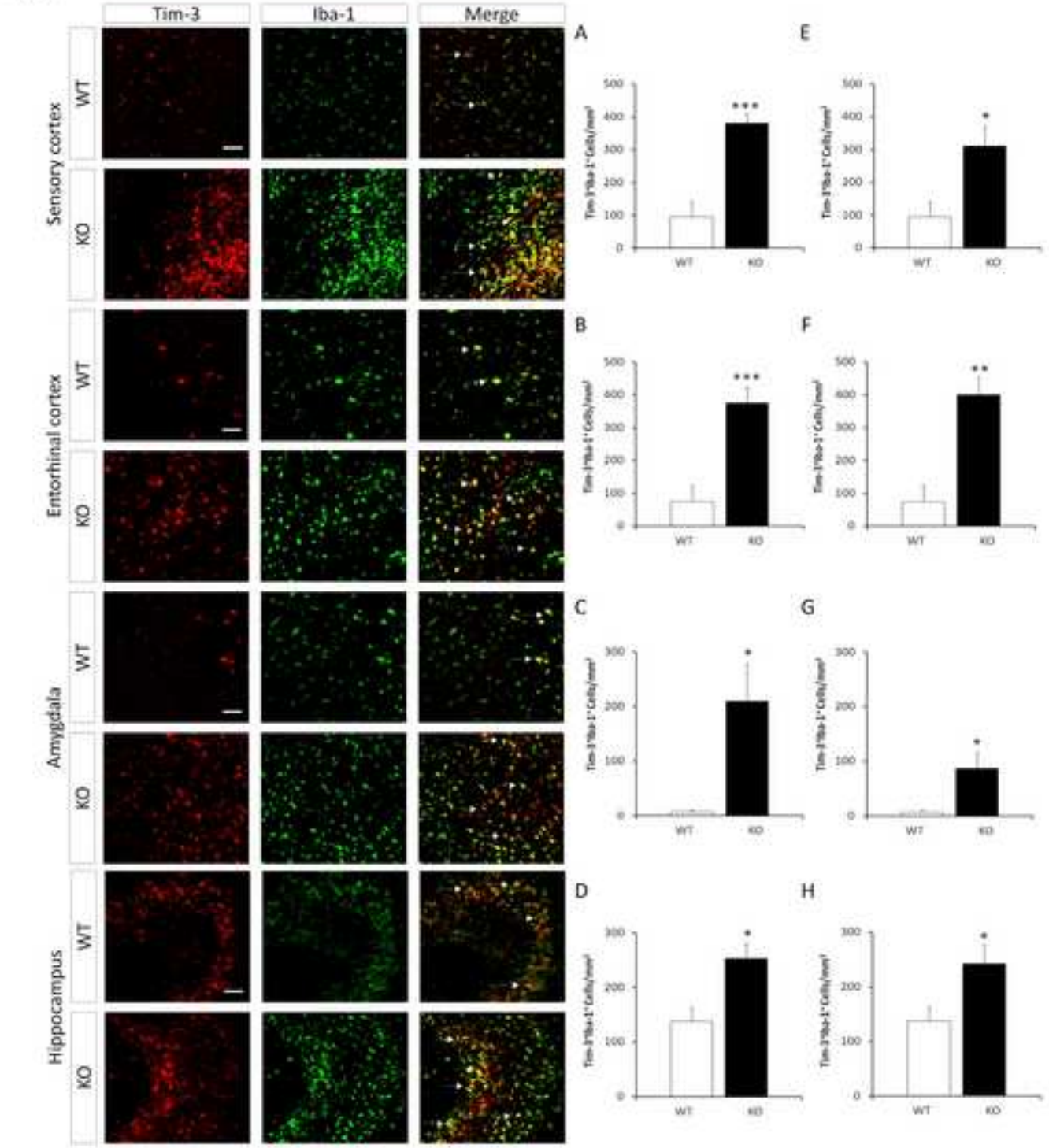

Figure 7

Click here to download high resolution image

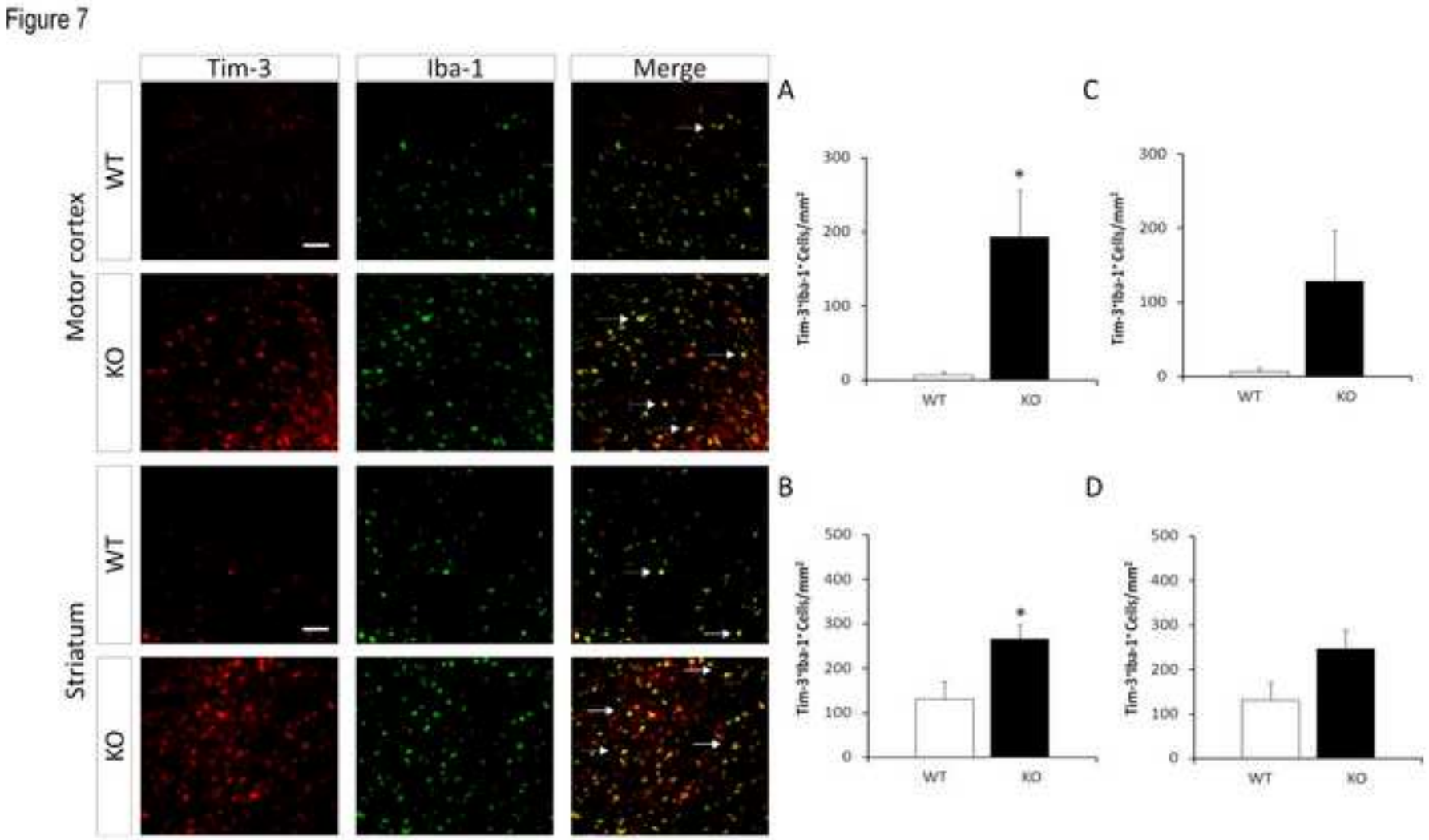

Figure 8

Click here to download high resolution image

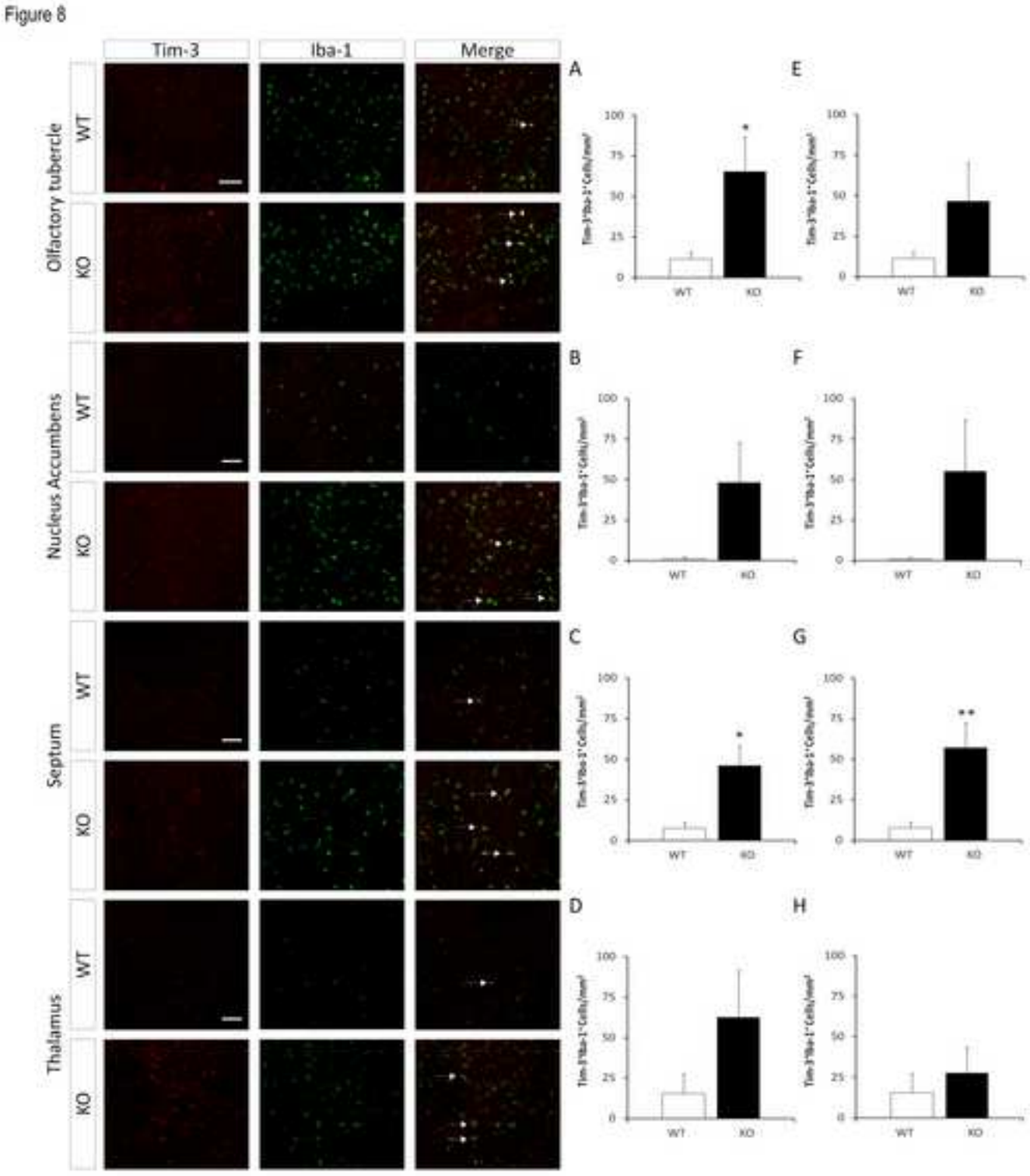

Figure 9

Click here to download high resolution image

Figure 9

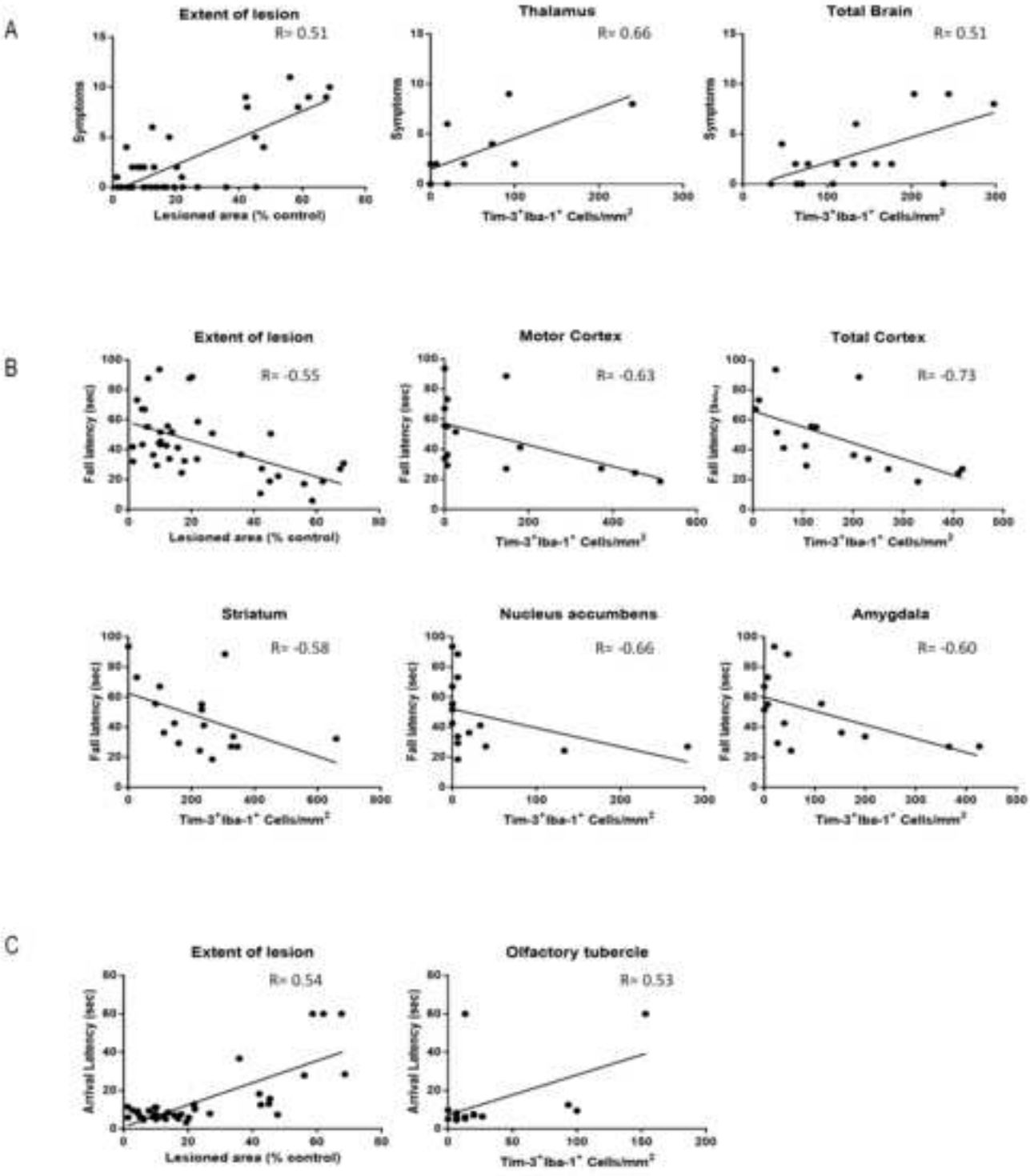

Role of the Funding Source

This work was supported by the Marató TV3 Foundation (#111832), the "Instituto de Salud Carlos III" (RETICS-RTA, #RD12/0028/0023), the "Generalitat de Catalunya", "ICREA Acadèmia" (2015) and "AGAUR" (#2014-SGR-1547) to R.M. None of them had a role in study design; in the collection, analysis and interpretation of data; in the writing of the report; and in the decision to submit the paper for publication

Contributors

PR and RM participated in the design and coordination of the study, analysed the data, and contributed to the writing of the manuscript. EK performed experiments, analysed the data, and helped to draft the manuscript. All authors read and approved the final manuscript.

***Conflict of Interest**

Competing interests

The authors declare that they have no competing interests.

Acknowledgements

We would like to thank Sevcan Cigerli, Alex Clayton-Marucci, Marta Linares and Dulce Real for technical support.

Highlights

Click here to download Supplementary Material: Highlights.docx

Table 1

Click here to download Supplementary Material: Supp Table 1.docx

Supp Figure 1

Click here to download Supplementary Material: SUPP FIG 1.tif